Title Page

Title: A concept shift in the mechanistic understanding of HIFα-regulated developmental myelination.

Running Title: Mechanisms of HIFα-regulated myelination

Author name: Sheng Zhang, Yan Wang, Bokyung Kim, and Fuzheng Guo

Author affiliation: Department of Neurology, School of Medicine, The University of California, Davis; The Institute for Pediatric Regenerative Medicine (IPRM), Shriners Hospitals for Children, Northern California.

Corresponding author: Fuzheng Guo, PhD, 2425 Stockton Blvd, Sacramento, CA 95817. Email: fzguo@ucdavis.edu ORCID: 0000-0003-3410-8389

Number of pages: 46

Number of Figures: 12

Competing interests: The authors declare no competing financial interests

Number of words: Abstract, 210, Introduction, 498, Discussion, 1475

Acknowledgements: This study was supported by the grants funded by NIH/NINDS (R21NS109790 and R01NS094559 to F.G.) and Shriners Hospitals for Children (86100, 85200-NCA16, 85107-NCA-19 to F.G., 84307-NCAL to S.Z.,).

Abstract (210 words)

The developing CNS is exposed to physiological hypoxia, under which hypoxia inducible factor alpha (HIFα) is stabilized and plays a crucial role in regulating neural development. The cellular and molecular mechanism of HIFα in developmental myelination remain incompletely understood. Previous concept proposes that HIFα regulates CNS developmental myelination by activating the autocrine Wnt/β-catenin signaling in oligodendrocyte progenitor cells (OPCs). Here, by analyzing a battery of genetic mice of both sexes, we presented *in vivo* evidence supporting an alternative understanding of oligodendroglial HIFα-regulated developmental myelination. At the cellular level, we found that HIFα was required for developmental myelination by transiently controlling upstream OPC differentiation but not downstream oligodendrocyte maturation and that HIFα dysregulation in OPCs but not oligodendrocytes disturbed normal developmental myelination. We demonstrated that HIFα played a minor, if any, role in regulating canonical Wnt signaling in the oligodendroglial lineage or in the CNS. At the molecular level, blocking the autocrine Wnt signaling did not affect HIFα-regulated OPC differentiation and myelination. We further identified HIFα-Sox9 regulatory axis as an underlying molecular mechanism in HIFα-regulated OPC differentiation. Our findings support a concept shift in our mechanistic understanding of HIFα-regulated CNS myelination from the previous Wnt-dependent view to a Wnt-independent one and unveil a previously unappreciated HIFα-Sox9 pathway in regulating OPC differentiation.

Significant statement (100 words)

Promoting disturbed developmental myelination is a promising option in treating periventricular leukomalacia, a major form of brain white matter injury affecting premature infants. In the developing CNS, HIFα is a master regulator that adapts neural cells to physiological and pathological hypoxic cues. The role and mechanism of HIFα in oligodendroglial myelination, which is developmentally disturbed in preterm infants affected with

periventricular leukomalacia, are incompletely understood. Our findings presented here represent a concept shift in our mechanistic understanding of HIFα-regulated developmental myelination and suggest the potential of intervening oligodendroglial HIFα-mediated signaling pathway in mitigating disturbed myelination in premature white matter injury.

Introduction (**498 words**)

HIFα is a master transcriptional regulator of the adaptive response to hypoxia (Semenza, 2012). Under the physiological state, the oxygen concentration in the developing CNS was reported ranging from 0.5 to 7% (Ivanovic, 2009; Zhang et al., 2011). HIFα protein (HIF1α and HIF2α) is constitutively translated but subjected to rapid turnover (half-life<5 min) by the proteasome-mediated degradation in which the von Hippel-Lindau (VHL) protein plays an essential role (Semenza, 2012). Under physiological or pathological hypoxia or VHL mutation, HIFα accumulates in the nucleus where it complexes with the stable HIFβ subunit and the co-activator P300/CBP to activate the signaling target gene expression.

The role of HIFα, particularly the representative HIF1α, in neural precursor cells under physiological conditions has been extensively investigated (Cunningham et al., 2012; Li et al., 2014; Milosevic et al., 2007; Tomita et al., 2003). Aggravated hypoxia and/or ischemia causes severe disturbance of normal oligodendroglial myelination in the preterm infants born between 28th and 37th week gestational ages (Volpe, 2009). Animal studies demonstrate that pathological hypoxia insult delays developmental myelination in preterm-equivalent early postnatal murine CNS (Jablonska et al., 2012; Liu et al., 2011; Liu et al., 2013). The role of HIFα in developmental myelination has not been defined until an important study reported that HIFα plays a major role in hypoxia-elicited myelination disturbance in the cell/brain slice culture systems (Yuen et al., 2014). However, the underlying cellular and molecular mechanisms of oligodendroglial HIFα-regulated myelination remain incompletely defined. The current popular hypothesis states that HIFα dysregulation disturbs developmental myelination by activating autocrine Wnt/β-catenin signaling (Yuen et al., 2014). This “Wnt-dependent” mechanistic

hypothesis is in line with the inhibitory effect of intracellular Wnt/β-catenin activation on CNS myelination (Guo et al., 2015), but it was only tested in the cell / slice culture systems in combination with pharmacological manipulations. Given the intrinsic caveats of cellular non-specificity and/or off-target effect of pharmacological application, it is imperative to determine, by using *in vivo* genetic approaches, the involvement of oligodendroglial HIFα-derived Wnt signaling in developmental myelination.

CNS developmental myelination consists of at least two major sequential steps: OPC differentiation into oligodendrocytes (OLs, referred to as OPC differentiation) and oligodendrocyte maturation (Guo et al., 2015; Huang et al., 2013). In humans, developmental myelination starts in the third trimester of gestational ages, which is equivalent to the perinatal and early postnatal ages in rodents (Semple et al., 2013). Therefore, we used the murine CNS of perinatal and early postnatal ages as a third trimester-equivalent *in vivo* model to dissect the cellular and molecular mechanisms of HIFα underlying development myelination. By analyzing a series of cell-specific HIFα and Wnt genetic mutant mice, we provided convincing evidence supporting an alternative HIFα model of CNS myelination: endogenous HIFα transiently regulates developmental myelination by controlling upstream OPC differentiation but not downstream OL maturation and its hyperactivation disturbs OPC differentiation in a manner independent of autocrine Wnt/β-catenin signaling. Our results further demonstrate that sustained Sox9 activation is a downstream mechanism underlying disturbed OPC differentiation elicited by HIFα hyperactivation.

Materials and Methods

Transgenic animals: The following transgenic mice were used in our study: *Cnp-Cre* mice (RRID: MGI_3051754) were kindly provided by Dr. Nave (Lappe-Siefke et al., 2003), *Sox10-Cre* (RRID: IMSR_JAX:025807), *Sox10-CreER*^{T2} (RRID:IMSR_JAX: 027651) , *Pdgfrα-CreER*^{T2} (RRID: IMSR_JAX:018280) , *Hif1α*-floxed (RRID: IMSR_JAX:007561), *Hif2α*-floxed (RRID: IMSR_JAX:008407), *Vhl*-floxed (RRID: IMSR_JAX:012933), *Wls*-floxed (RRID:

IMSR_JAX:012888). All mice were maintained on the C57BL/6 background and housed in 12 h light/dark cycle with free access to water and food. Animal protocols were approved by the Institutional Animal Care and Use Committee at the University of California, Davis.

Tamoxifen treatment: Tamoxifen (TM) (T5648, Sigma) was prepared at a concentration of 30 mg/ml in a mixture of ethanol and sunflower seed oil (1:9, v/v). All study mice including non-Cre Ctrl and conditional knockout were received tamoxifen intraperitoneally at a dose of 200 µg/g body weight.

Hypoxia/ischemia (H/I)-induced brain white matter injury: We used the established protocol (Shen et al., 2010) to induce H/I injury in C57BL/6J background mice at postnatal day 6 (P6), a time point when OPC differentiation barely occurs. In brief, P6 mice were anesthetized with indirect cooling by wet ice, which were immediately subjected to permanent occlusion (by cauterizers) of the right side common carotid artery (ischemia). One hour after the artery occlusion, mice were exposed to 6% O_2 for 45min (hypoxia). After hypoxia exposure, the mice were returned to the dam. Previous study demonstrates that H/I injury results in widespread periventricular white matter injury including arrested OPC differentiation and microglial/astroglial activation (Liu et al., 2011).

Tissue processing and immunohistochemistry: After anesthetization by ketamine/xylazine mixture, mice were perfused with cold PBS. Tissues were collected, fixed with fresh 4% PFA for 2 h at room temperature, cryopreserved in 30% sucrose overnight at 4°C and embedded in OCT (VWR International, Wetzlar, Germany). Serial coronal sections (14 µm) were cut by a Leica Cryostat (CM 1900-3-1). Tissue sections were incubated with primary antibody overnight at 4°C after blocking with 10% donkey serum at room temperature for at least 1 h. After 3 times wash, the fluorescence conjugated secondary antibody (Jackson ImmuneResearch) was applied and incubated for 1.5 h. Then the slice was protected by mounting medium after DAPI nucleus staining. The following primary antibodies were used in immunohistochemical study:

HIF-1α (RRID:AB_409037,1:200,Cayman Chemical #100642,), Sox10 (RRID: AB_2195374,1:100,Santa Cruz Biotechnology, sc-17342; RRID: AB_778021, 1:500, Abcam, ab27655), Olig2 (RRID: AB_570666,1:200, Millipore, AB9610), Mbp (RRID:AB_2564741, 1:500, Biolegend, SMI-99,), SMI312 (RRID:AB_2135329, 1:1000, Covance, SMI-312R), CC1 (RRID:AB_213434, 1:200, Calbiochem, OP80,), PDGFRα (RRID:AB_2236897,1:200, R&D system, AF1062), SMI32 (RRID:AB_2314912, 1:1000, Biolegend, SMI-32P), Sox9 (RRID:AB_2194160,1:200, R&D system, AF3075).

In situ hybridization and transmission electron microscopy (TEM): Briefly, the slices were treated with Proteinase K (Thermo Fisher, AM2548) and acetylated by triethanolamine (Sigma, 90279) and acetic anhydride (Sigma, 320102). The tissue was incubated with 100 ng/ul DIG labelled c-RNA at 65^0C overnight. Then the slices were incubated with Alkaline phosphatase (AP) anti-DIG secondary antibody (1:100,11093274910, Sigma) overnight after blocking with 10% donkey serum. The signal was determined by nitroblue tetrazolium (NBT) and 5-bromo-4-chloro-3-indolyl phosphate (toluidine salt) (BCIP) (Sigma, 72091).Semithin sections for toluidine blue myelin staining and ultrathin section for TEM imaging were prepared according to our previous protocols (Zhang et al., 2018a; Zhang et al., 2018b). TEM imaging was conduction by the professionals at UC Davis Core Facility who were blinded to the mouse genotypes.

Enzyme-linked immunosorbent assay (ELISA): The Wnt3a protein level was measured by the mouse Wnt3a ELISA kit (M13146365, CSB-EL026136MO, Cusabio) according to the manufacturer's instruction.

Primary OPC culture and gene manipulation: The mouse cortex between P0 and P2 was collected and dissociated with papain kit and DNase I (#LK003176, Worthington; 250U/ml; #D5025, Sigma). OPCs were purified by immnopanning approach according to our previous protocol (Lang et al., 2013). Purified OPCs were used for experiments of Wls knockdown, Wnt3a overexpression, and Sox9 overexpression. Wls-shRNA (TRCN 0000 234932, Mission ShRNA bacterial Glycerol stock NM_026582) and scramble control (Mission TRC2 PlkO.5-

PURO Non-Mammalian shRNA control Plasmid) were purchased from Sigma-Aldrich. Wnt3a plasmid pLCN-Wnt3a-HA (Addgene, #18030) and empty pLCN-exp (Addgene, #64865) were used for Wnt3a overexpression experiment. The transfection of Wls-shRNA and pLCN-Wnt3a-HA and controls was performed by using HiPerFect transfection reagent (#301704, Qiagen) according to the manual. p-WPXL-Sox9 (Addgene, #36979) and control plasmid p-WPXL (Addgene, #12257) were used for Sox9 overexpression and the transfection was performed by using FuGENE6 Transfection reagent (Promega, #E2691, lot#000371257).

Primary rat OPCs were used in Sox9 knockdown and DMOG treatment. DMOG (0.5 mM dissolved in DMSO, D3695, Sigma), and Sox9 siRNA (SASI_Rn02_00372739, Sigma) or negative control siRNA (SIC001-5X1NMOL, Sigma) were applied according to the experimental design in Figure 12H. Transfection of Sox9 siRNA was conducted by using HiPerFect transfection reagent (#301704, Qiagen).

Purification of brain OPCs by magnetic activated cell sorting (MACS): MACS purification of OPCs was performed according to the protocols in the kit instruction from Miltenyi Biotec. The mouse forebrain was dissociated using the papain dissociation system (LK003176, Worthington) and gentleMACS^{TM} Dissociator (Miltenyi Biotec, #130-092-235). Astrocytes and microglia in the cell suspension were removed by using anti-ACSA-2 micro beads (130-097-679, Miltenyi Biotec) and anti-CD11b micro beads (130-049-601, Miltenyi Biotec), respectively. After astroglial and microglial removal, the cell suspension was then incubated with anti-O4 micro beads (130-094-543, Miltenyi Biotec) for OPC purification. $O4^+$ cells were collected for RNA preparation.

RNA preparation, reverse transcription and real-time quantitative PCR (RT-qPCR): Total RNA was obtained using Qiagen RNeasy for lipid tissue kit (74804, Qiagen) according to the manual. We used on-column DNase I digestion to eliminate DNA contamination. Complementary DNA (cDNA) was prepared using Qiagen Omniscript RT Kit (205111, Qiagen). Mouse and rat gene expression was normalized to the internal control Hsp90 and β-actin,

respectively, and calculated by the equation of $2^{(Ct(cycle\ threshold)\ of\ Hsp90\ -\ Ct\ of\ indicated\ genes)}$. The value of control groups was normalized to 1 throughout the study. Real time qPCR was done by using QuantiTect SYBR® Green PCR Kit (204145, QIAGEN) and Strategene MP3005P thermocycler. The qPCR primers used in the study were shown as below.

Mouse Wls: AGGGCAAGGAAGAAGGAGAG / ATCCCTCCAACAATGCAGAG

Mouse Glut1: CAGTTCGGCTATAACACTGGTG / GCCCCCGACAGAGAAGATG

Mouse Ldha: CATTGTCAAGTACAGTCCACACT / TTCCAATTACTCGGTTTTTGGGA

Mouse Hk2: TGATCGCCTGCTTATTCACGG / AACCGCCTAGAAATCTCCAGA

Mouse Axin2: AACCTATGCCCGTTTCCTCTA / GAGTGTAAAGACTTGGTCCACC

Mouse Naked1: CAGCTTGCTGCATACCATCTAT / GTTGAAAAGGACGCTCCTCTTA

Mouse Wnt7a: CGACTGTGGCTGCGACAAG / CTTCATGTTCTCCTCCAGGATCTTC

Mouse Wnt7b: CTTCACCTATGCCATCACGG / TGGTTGTAGTAGCCTTGCTTCT

Mouse Vegfa: GCACATAGAGAGAATGAGCTTCC / CTCCGCTCTGAACAAGGCT

Mouse Mbp: ACACGAGAACTACCCATTATGGC / CCAGCTAAATCTGCTGAGGGA

Mouse Plp (exon3b-specific): CCAGAATGTATGGTGTTCTCCC / GGCCCATGAGTTTAAGGACG

Mouse Cnp: TTTACCCGCAAAAGCCACACA / CACCGTGTCCTCATCTTGAAG

Mouse Mobp: AACTCCAAGCGTGAGATCGT / CAGAGGCTGTCCATTCACAA

Mouse Opalin: CTGCCTCTCACTCAACATCA / GCTGGATCAAAGTAAACAGC

Mouse Mog: AGCTGCTTCCTCTCCCTTCTC / ACTAAAGCCCGGATGGGATAC

Mosue Qk: CTGGACGAAGAAATTAGCAGAGT / ACTGCCATTTAACGTGTCATTGT

Mouse Myrf: CAGACCCAGGTGCTACAC / TCCTGCTTGATCATTCCGTTC

Mouse Sox9: AGTACCCGCATCTGCACAAC / ACGAAGGGTCTCTTCTCGCT

Mouse Hsp90: AAACAAGGAGATTTTCCTCCGC / CCGTCAGGCTCTCATATCGAAT

Rat Bnip3: GCTCCCAGACACCACAAGAT / TGAGAGTAGCTGTGCGCTTC

Rat Mbp: TTGACTCCATCGGGCGCTTCTTTA / TTCATCTTGGGTCCTCTGCGACTT

Rat Sox9: CTGAAGGGCTACGACTGGAC / TACTGGTCTGCCAGCTTCCT

Rat β-actin: CGTCTTCCCCTCCATCGT / GGAGTCCTTCTGACCCATACC

Chromatin immunoprecipitation (ChIP) by HIFα antibody and qPCR verification: ChIP was performed using the SimpleChIP plus Enzymatic Chromatin IP kit (Cell Signaling Technology, #9005) following the manufacturer's protocol with some modifications. Briefly, primary cultured rat OPCs (4 x 10^6 cells) treated with 1 mM DMOG for 7 hours were crosslinked in culture medium containing 1% formaldehyde at room temperature for 10 min. After addition of glycine solution to stop the reaction, the cells were then collected, centrifuged and lysed. Nuclei were collected and treated with 0.5 ul micrococcal nuclease per IP for 20 min at 37 °C. The reaction was stopped using 0.05 M EDTA, and nuclear membranes were destroyed by sonication. Then the supernatant was collected by centrifugation. Chromatin solutions were incubated with 10 ug of anti-HIF1α (Cayman, Rabbit, #10006421) antibody or anti-rabbit IgG (Cell Signaling #2729) overnight at 4 °C, and immunoprecipitated with protein G magnetic beads for 2 hours at 4 °C with rotation. Bound DNA-protein complexes were washed and eluted, and crosslinks were reversed according to kit instructions. DNA was purified using spin columns and used for ChIP-qPCR analysis. The fold enrichment of specific genomic regions was assessed relative to the qPCR data from the IPs normalized to the control IgG values. Fold enrichment = $2^{\wedge -[(Ct\ IP) - (Ct\ IgG)]}$.
qPCR primer sets for ChIP binding site verification are:

Negative site: forward TTCCTCTTGGGATGGTTGTC / reverse CCACCTCTGGGGAGTATGAA

-75bp site: forward TTTCAAAATCCGGTCCAATC / reverse CCCCCTTCACCTTAGAGACC

-828bp site: forward CGGGGAAGGACTTGTCAGT / reverse ATGAAAACCAAAGCCAAGCA

-1211bp site: forward CGGCTCCAAGCACTCTTAAA /reverse GCGTCCTTTTAGACCTGCAC

-1928 site: forward GTCGTTCTCGCTGCCTTTAG / reverse TTGAAGAGACCAGGGACCAC

-2098 site: forward CTCTGGATGTTGCCGAAAAT / reverse CTCCACGCAAGCGTTTTTAT

Western blot and antibodies: Twenty microgram protein was loaded into AnykD Mini-PROTEAN gel (#4569035, BIO-RAD). After blocking, the membrane was incubated with primary antibodies overnight. The membrane was washed 3 times by TBST (TBS with 1% tween 20). Then the HRP-conjugated secondary antibody was reacted with membrane for 1.5 hours. Protein signals were developed by using ECL kit (NEL103001EA, Perkin Elmer). Quantification of interested protein bands were conducted by using NIH Image J software. Antibodies used in western blot are MBP (SMI-99, RRID:AB_2564741, 1:2000, Biolegend), Active β-catenin (#05-665, RRID: AB_309887, 1:1000, Millipore), Axin-2(#6163, RRID: AB_10904353, 1:1000, Prosci) and β-actin (3700, RRID:AB_2242334, 1:2000, Cell signaling Technology).

Experimental design and statistical analyses: Data collection was conducted by lab members who were blinded to mouse genotypes. We used Shapiro-Wilk approach to test data normality. F test and Browne-Forsythe test were used to variance equality of two groups and three or more groups, respectively. We used scatter graphs to present the quantification data throughout the current manuscript. Both male and female mice were included in our data analysis. All data were presented as mean ± standard effort of mean (s.e.m.) where each dot represents one mouse. Unpaired two-tailed Student's t test was used for statistically analyzing two groups of data where the *t*-values and the degree of freedom (df) were shown as $t_{(df)}$ in each graph. One-way ANOVA followed by Tukey's post test was used for statistically analyzing three or more groups of data. The F ratio, and DFn and DFd was presented as F(DFn, DFd) in the figure legends where DFn stands for degree of freedom numerator and DFd for degree of freedom of denominator. The exact P-value of one-way ANOVA test was also described in the figure legends. All data graphing and statistical analyses were performed using GraphPad Prism version 8.0. The P-value was designated as * $P<0.05$, ** $P<0.01$, *** $P<0.001$, ns, not significant $P>0.05$.

Results

Disrupting HIFα in OPCs but not OLs delays developmental myelination

HIF1α and HIF2α share high sequence homology and function in a similar manner through partnering with HIF1β and subsequently activating HIFα target genes (Semenza, 2012). Therefore, we used antibody against the representative HIF1α to determine whether endogenous HIFα protein is stabilized in the perinatal and early postnatal CNS, where the vasculature is still in immature state (Harb et al., 2013; Yuen et al., 2014). We found that HIF1α signals were detected in Sox10^{+} oligodendroglial lineage cells in the white matter areas of the spinal cord (**Fig. 1A**) and the forebrain (**Fig. 1C**) at postnatal day 5 (P5). As positive controls, HIF1α immunoreactive signals were markedly increased in age-matched transgenic *Sox10-Cre:Vhl*$^{fl/fl}$ mice (**Fig. 1B, D**), in which *Sox10-Cre*-mediated VHL disruption prevents HIFα from degradation specifically in oligodendroglial lineage cells. HIF1α signals became barely detectable in the forebrain white matter at P10 but substantially upregulated in mice that had been challenged by hypoxia/ischemia insults at P6 (**Fig. 1E**) (Liu et al., 2011; Shen et al., 2010). These immunohistochemical results demonstrate that HIFα is transiently stabilized in the early postnatal CNS and rapidly downregulated in the second postnatal week and that hypoxia/ischemia injury results in sustained HIFα stabilization in the brain white matter.

To define the role of physiological HIFα stabilization in developmental myelination, we used *Cre-loxP*-based genetic approach to conditionally disrupt HIFα function. Previous studies have demonstrated that *Pdgfrα-CreER*^{T2} drives gene disruption in OPCs whereas *Cnp-Cre* in later stages of oligodendrocyte development (Moyon et al., 2016; Zhang et al., 2018a; Zhang et al., 2018b). Our extensive analysis of HIF1α or HIF2α conditionally knockout mice driven by *Pdgfrα-CreER*^{T2} and *Cnp-Cre* revealed no phenotypic abnormalities of the oligodendroglial lineage, suggesting functional redundancy between HIF1α and HIF2α. We therefore generate HIF1α and HIF2α double conditional knockout (referred to as HIFα cKO).

To determine the role of HIFα in OPC differentiation, we used *Pdgfrα-CreER*^{T2}:*Hif1α*$^{fl/fl}$:*Hif2α*$^{fl/fl}$ (PDGFRα:HIFα cKO) transgenic mice. Tamoxifen was administered to

PDGFRα:HIFα cKO and non-Cre littermate control (*Hif1α*$^{fl/fl}$:*Hif2α*$^{fl/fl}$) pups at P1, P2, and P3 and the CNS tissue was analyzed at P8. Our previous data show that this tamoxifen paradigm induces ~90% of gene cKO efficiency in OPCs (Zhang et al., 2018a; Zhang et al., 2018b). The density of differentiated OLs but not OPCs was significantly decreased in the spinal cord white matter of PDGFRα:HIFα cKO mice compared with non-Cre littermate controls (**Fig. 2A-B**), suggesting that HIFα is dispensable for OPC population expansion and but required for OPC differentiation. In agreement of OPC differentiation inhibition, the mRNA levels of major myelin protein (MBP and PLP) and mature OL-enriched protein (Opalin and QK, aka CC1) were significantly reduced in PDGFRα:HIFα cKO mice compared with non-Cre littermate controls (**Fig. 2C**). In the forebrain, developmental myelination in the periventricular white matter was delayed in PDGFRα:HIFα cKO mice at P8 (**Fig. 2D**) and became indistinguishable from that in littermate control mice at P14 (**Fig. 2E**). These data suggest that HIFα regulates the timing of developmental myelination.

To determine the role of HIFα in oligodendroglial maturation, we used *Cnp-Cre*:*Hif1α*$^{fl/fl}$:*Hif2α*$^{fl/fl}$ (Cnp:HIFα cKO) and non-Cre littermate control (*Hif1α*$^{fl/fl}$:*Hif2α*$^{fl/fl}$) mice. The expression of the typical HIFα target gene *Ldha* and *Vegfa* (Sharp and Bernaudin, 2004) was significantly reduced in Cnp:HIFα cKO mice (**Fig. 2F**), thus validating the disruption of HIFα function. Unexpectedly, we found no significant difference in developmental myelination (**Fig. 2G**), the number of OLs (**Fig. 2H**) and OPCs (**Fig. 2I**), and myelin gene expression (**Fig. 2J**) between Cnp:HIFα cKO and non-Cre littermate controls mice at different ages (P2, P8, and P14). These data indicate that HIFα plays no roles in oligodendrocyte maturation. Taken together, the contrast phenotypes derived from PDGFRα:HIFα cKO vs Cnp:HIFα cKO mice support a working model that HIFα controls the timing of developmental myelination by regulating upstream OPC differentiation but not downstream oligodendrocyte maturation.

Disrupting oligodendroglial HIFα does not affect axonal integrity or cell survival.

HIFα is required for neuronal survival, as HIFα deficiency in Nestin-expressing neural cells results in massive neuronal death (Tomita et al., 2003). Recent data reported that HIFα deficiency in Olig1-expressing neural cells leads to neuronal death and widespread axonal injury in the corpus callosum at the perinatal ages (Yuen et al., 2014). To determine whether OPC or OL-specific HIFα deficiency causes axonal damage and cell death, we employed IHC of SMI32, which labels functionally compromised axons (Yuen et al., 2014) and a subset of pyramidal neuronal cell bodies and dendrites (Campbell and Morrison, 1989; Haynes et al., 2005; Voelker et al., 2004) (**Fig. 3A**, Ctx), and cleaved Caspase 3 (CC3), which labels apoptotic cells. We did not observe SMI32 immunoreactive signals in the corpus callosum of Cnp:HIFα cKO (**Fig. 3A**) and PDGFRα:HIFα cKO (**Fig. 3C**) mice compared with respective littermate controls. In contrast, many tightly packed axons running through the corpus callosum were clearly labeled by the pan-axonal marker SMI312 (**Fig. 3B, D**). Furthermore, the densities of $CC3^+$ apoptotic cells and $CC3^+/Sox10^+$ apoptotic oligodendroglial lineage cells were statistically indistinguishable between PDGFRα (or Cnp):HIFα cKO mutants and their respective littermate controls (**Fig. 3E-G**). Thus, disrupting oligodendroglial HIFα does not affect neuronal cell survival and axonal integrity in the white matter in the early postnatal CNS.

HIFα hyperactivity impairs OPC differentiation but not oligodendrocyte maturation

Pathological hypoxia-ischemia insults caused aberrant HIFα stabilization in the white matter (**Fig. 1E**). To determine whether aberrant HIFα stabilization disturbs normal developmental myelination, we induced HIFα hyperactivity by conditionally disrupting the negative regulator VHL (**Fig. 1B, D**). Constitutive *Sox10-Cre:Vhl*$^{fl/fl}$ (Sox10:VHL cKO) mice were much smaller than non-Cre littermate controls (*Vhl*$^{fl/+}$, or *Vhl*$^{fl/fl}$) at birth and rarely survived beyond P7. Our data show that *Sox10-Cre*-mediated gene disruption occurs in early OPCs during embryonic CNS development (Zhang et al., 2018a). *Sox10-Cre*-elicited HIFα hyperactivity (cf **Fig. 6A**) caused severe hypomyelination in the spinal cord (**Fig. 4A**). Quantification data showed that the number of differentiated OLs (**Fig. 4B, C**) and the mRNA

level of major myelin protein (**Fig. 4D**) were reduced by 40-60% in Sox10:VHL cKO mutants compared with non-Cre littermate controls. However, the number of OPCs was unaffected in Sox10:VHL cKO mutants (**Fig. 4C**). The observation of hypomyelination, decreased OL number, and unaffected OPC number was confirmed by employing inducible *Sox10-CreER*^{T2}:*Vhl*$^{fl/fl}$ (iSox10:VHL cKO) (cf **Fig. 9**) and *Pdgfrα-CreER*^{T2}*:Vhl*$^{fl/fl}$ (PDGFRα:VHL cKO) mutants (**Fig. 5**) in which HIFα was stabilized in postnatal OPCs by tamoxifen treatment at neonatal ages of P1, P2, and P3. Thus, our *in vivo* data derived from three different genetic mouse models suggest that HIFα hyperactivity disturbs developmental myelination by inhibiting OPC differentiation.

To determine the effect of HIFα hyperactivation on oligodendrocyte maturation, we analyzed *Cnp-Cre:Vhl*$^{fl/fl}$ (Cnp:VHL cKO) mutants. Cnp:VHL cKO mice were viable and indistinguishable from non-Cre littermates throughout the early postnatal and adult ages. In sharp contrast to OPC-specific VHL cKO, Cnp:VHL cKO mice had normal levels of myelin gene expression (**Fig. 4E, F, H**), unperturbed myelination (**Fig. 4G**), and normal numbers of OLs and OPCs (**Fig. 4I**) despite the elevated density of blood vessels in the CNS that we previously reported (Guo et al., 2015). These data indicate that HIFα hyperactivation in OLs does not affect their maturation. Taken together, our genetic evidences convincingly demonstrate elevated HIFα activity perturbs developmental myelination by inhibiting OPC differentiation but not OL maturation, suggesting a lineage stage-dependent role of HIFα in developmental myelination.

Oligodendroglial HIFα play minor roles, if any, in regulating Wnt/β-catenin signaling activity.

Previous study reported that aberrant HIFα stabilization in OPCs activates Wnt7a/Wnt7b expression and canonical Wnt (i.e. Wnt/β-catenin) signaling (Yuen et al., 2014). However, the unbiased RNA-seq analysis of *Sox10-Cre:Vhl*$^{fl/fl}$ mice prompted us to revisit HIFα-Wnt regulation in oligodendroglial lineage cells (**Fig. 6A-E**). Sox10-Cre-mediated VHL cKO markedly elevated HIFα activity, as evidenced by increased expression of the typical HIFα target genes *HK2, Ldha,*

Glut1, Bnip3, and *Vegfa* (**Fig. 6A**). In stark contrast to HIFα hyperactivation, there were no significant changes in the expression of the Wnt genes of *Wnt7a* and *Wnt7b* and the canonical Wnt signaling target genes of *Axin2* and *Naked1* and (**Fig. 6B**). The KEGG pathway of HIF-1 signaling and the GO term of response to hypoxia were significantly overrepresented amongst 255 upregulated genes (**Fig. 6C, D**) whereas the GO terms of oligodendrocyte differentiation and sterol biosynthesis were significantly overrepresented amongst 351 downregulated genes (**Fig. 6E**), which is in agreement with elevated HIFα signaling and diminished OPC differentiation in the CNS of Sox10:VHL cKO mice we documented in **Fig. 4A-D**. However, we did not find overrepresentation of Wnt-related KEGG pathways or GO terms amongst the differentially regulated genes. The unbiased analysis of gene regulation at the transcriptomic level strongly suggests that oligodendroglial HIFα stabilization plays no roles in regulating canonical Wnt signaling.

To strengthen our conclusion derived from RNA-seq, we analyzed OPCs isolated from PDGFRα:VHL cKO mice. Tamoxifen was injected to PDGFRα:VHL cKO and littermate control mice at P5 and brain OPCs were acutely purified at P6 by magnetic activated cell sorting (MACS) approach (**Fig. 6F**). As shown in **Fig. 6G**, HIFα function was indeed stabilized in purified VHL-disrupted OPCs, as evidenced by elevated expression of the HIFα target gene *Hk2, Ldha*, and *Glut1*. However, there were no significant changes in the expression of the Wnt/β-catenin signaling target genes *Axin2* and *Naked1* and the Wnt ligand genes *Wnt7a* and *Wnt7b* in VHL-disrupted OPCs compared with VHL-intact OPCs (**Fig. 6H**), suggesting that genetically stabilizing HIFα does not perturb the autocrine Wnt/β-catenin signaling activity or the expression of Wnt7a and Wnt7b in OPCs.

To corroborate our findings, stabilizing HIFα in PDGFRα^{+} OPCs did not affect the activity of Wnt/β-catenin activity in the spinal cord at P8 (tamoxifen at P1, P2, and P3) and in the forebrain at P14 (tamoxifen at P6 and P7) of PDGFRα:VHL cKO mice compared with littermate controls, which was supported by unaltered expression of the Wnt target gene at mRNA and

protein levels (**Fig. 6I-J**). Our results further demonstrated that the expression of Axin2, Naked1, Wnt7a, and Wnt7b was not perturbed in PDGFRα:HIFα cKO mice compared with littermate controls (**Fig. 6K**). Thus, HIFα does not regulate the canonical Wnt signaling or Wnt7a/Wnt7b expression in the oligodendroglial lineage and in the CNS.

Blocking oligodendroglial-derived Wnt signaling does not affect HIFα hyperactivation-elicited inhibition of OPC differentiation and myelination.

That non-perturbation of the Wnt signaling in HIFα-stabilized OPCs led us to hypothesize that HIFα hyperactivation inhibits myelination in a manner independent of the autocrine Wnt activation in OPCs. To test our hypothesis, we stabilized HIFα function and simultaneously blocked oligodendroglial-derived autocrine Wnt signaling.

Previous studies demonstrated that disrupting WLS blocks the secretion of Wnt ligands from Wnt-producing cells and subsequently inhibits intracellular Wnt signaling activity in Wnt-receiving cells (Banziger et al., 2006; Bartscherer et al., 2006). To determine whether WLS deficiency blocks autocrine Wnt/β-catenin activity in OPCs, we knocked down WLS in Wnt3a-expressing primary OPCs (**Fig. 7A-C**). We chose Wnt3a because it is a typical Wnt ligand that activates the canonical Wnt signaling in Wnt-receiving cells. Wnt3a expression in OPCs significantly increased Wnt3a concentration and simultaneous WLS knockdown abrogated Wnt3a elevation in the culture medium of primary OPCs (**Fig. 7D**), suggesting that WLS is required for Wnt3a secretion from OPCs. We found that the activity of the canonical Wnt signaling, as assessed by the direct Wnt target gene *Axin2* and *Sp5*, was upregulated in Wnt3a-expressing OPCs but blocked in Wnt3a-expressing and WLS-deficient OPCs (**Fig. 7E, F**). These results demonstrate that disrupting WLS blocks OPC-derived autocrine Wnt/β-catenin signaling activity.

Genetically disrupting WLS in PDGFRα^{+} OPCs had no rescuing effects on HIFα hyperactivation-elicited hypomyelination (**Fig. 8A-C**), impaired OPC differentiation (**Fig. 8D-E**),

and diminished myelin gene expression (**Fig. 8F**) in PDGFRα:VHL/WLS cKO mice, suggesting that canonical Wnt signaling is unlikely a downstream pathway in mediating HIFα stabilization-induced inhibition of OPC differentiation. To corroborate this conclusion, we used a different inducible genetic model, *Sox10-CreER*^{T2}:*Vhl*$^{fl/fl}$:*Wls*$^{fl/fl}$ (iSox10:VHL/WLS cKO) (**Fig. 9A**). Conditionally stabilizing HIFα in Sox10-expressing oligodendroglial lineage cells resulted in hypomyelination and impaired OPC differentiation in iSox10:VHL cKO mice, however, simultaneous WLS cKO did not affect the degree of inhibited OPC differentiation and hypomyelination in iSox10:VHL/WLS cKO mice (**Fig. 9B-E**). We further demonstrated that disrupting WLS in Sox10-expressing oligodendroglial lineage cells had no detectable effect on normal OPC differentiation and developmental myelination in *Sox10-CreER*^{T2}:*Wls*$^{fl/fl}$ (iSox10:WLS cKO) mice compared with non-Cre littermate control mice (**Fig. 10**). Collectively, our results derived from cell-specific genetic approaches suggest that autocrine Wnt/β-catenin signaling plays a dispensable role in HIFα-regulated OPC differentiation and myelination.

HIFα stabilization activates Sox9 and sustained Sox9 activation mediates HIFα stabilization-elicited inhibition of OPC differentiation

The mRNA level of Sox9 was significantly upregulated in purified primary OPCs treated with dimethyloxalylglycine (DMOG), a potent HIFα stabilizer (Yuen et al., 2014), and this upregulation was abrogated upon simultaneous treatment of chetomin (**Fig. 11A**), an inhibitor of HIFα transcriptional activity (Kung et al., 2004; Viziteu et al., 2016), which suggests that HIFα may regulate Sox9 transcription. To support the functional regulation, our chromatin immunoprecipitation followed by qPCR assay (ChIP-qPCR) showed that HIFα physically bound to the promoter region (-828 bp) of the rat Sox9 gene (**Fig. 11B**). We found that Sox9 mRNA expression was significantly upregulated in the spinal cord of PDGFRα:VHL cKO mice compared with non-Cre littermate controls at P8 (**Fig. 11C**) and P14 (**Fig. 11D**). At the cellular level, sustained Sox9 expression was observed in HIFα-stabilized Sox10-expessing

oligodendroglial lineage cells in Sox10:VHL cKO mice (**Fig. 11E**, right, arrowheads), in sharp contrast to non-Cre control mice in which Sox9 was expressed at much lower level or barely detectable in Sox10-expressing cells (**Fig. 11E**, left, arrowheads). Our quantification showed that the percentage of Sox10$^+$ cells expressing Sox9 (**Fig. 11F**) and the level of Sox9 mRNA (**Fig. 11G**) were significantly increased in Sox10:VHL cKO mice. Furthermore, Sox9 expression was significantly elevated in primary OPCs, which were purified from Sox10:VHL cKO neonatal brain (**Fig. 11H**). These *in vitro* and *in vivo* data convincingly demonstrate that HIFα stabilization activates Sox9 expression in OPCs.

Recent data demonstrate that Sox9 is rapidly downregulated upon OPC differentiation (Reiprich et al., 2017), suggesting that sustained Sox9 expression may inhibits OPC differentiation. To this end, we overexpressed Sox9 in primary OPCs in growth medium and assess OPC differentiation in differentiating medium (**Fig. 12A**). Sox9 mRNA and protein were significantly increased in primary OPCs transfected with Sox9-expressing plasmid compared with those transfected with empty vector (EV) (**Fig. 12B-D**). Sox9 overexpression reduced the mRNA level of the most abundant myelin protein Plp and the potent pro-differentiation factor Myrf (Emery et al., 2009) assessed by RT-qPCR (**Fig. 12 E)**, the number of ramified MBP$^+$/Sox10$^+$ oligodendrocytes assessed by immunocytochemistry (**Fig. 12F**), and the protein level of MBP assessed by Western blot (**Fig. 12G**). To define the role of Sox9 activation in HIFα-regulated OPC differentiation, we stabilized HIFα in OPCs by DMOG treatment and simultaneously knocked down Sox9 expression by siRNA (**Fig. 12H-J**). Our data showed that Sox9 downregulation rescued the degree of myelin gene inhibition elicited DMOG treatment, as evidenced by the density of MBP$^+$/Sox10$^+$ differentiated OLs with ramified morphology (**Fig. 12K-L**) and the expression of myelin gene *Mbp* (**Fig. 12M**). Collectively, our results suggest that sustained Sox9 expression is one of the downstream molecular pathways in mediating HIFα-regulated OPC differentiation.

Discussion (1475 words)

Summary of key findings and conclusions

Through the extensive analysis of a series of HIFα genetic models, our study provides compelling evidences supporting an alternative understanding of the cellular and molecular mechanisms underlying HIFα-regulated CNS myelination (**Fig. 12N**). At the cellular level, HIFα regulates developmental myelination by controlling upstream OPC differentiation but not downstream oligodendrocyte maturation, which is supported by different responses of OPCs and oligodendrocytes to HIFα disruption and hyperactivation in regulating developmental myelination. At the molecular level, HIFα regulates OPC differentiation in a manner independent of the autocrine Wnt/β-catenin signaling. Instead, dysregulated Sox9 expression is one of the downstream pathways in mediating HIFα-regulated OPC differentiation (**Fig. 12N**).

HIFα regulates developmental myelination by controlling upstream OPC differentiation but not downstream oligodendrocyte maturation

One of the unexpected observations is the differential responses of OPCs and OLs to HIFα disruption and hyperactivation. Disrupting or stabilizing HIFα function results in severe disturbance of myelin gene expression and developmental myelination in the CNS of OPC-specific PDGFRα:HIFα (VHL) cKO mice. In sharp contrast, HIFα disruption or stabilization in Cnp:HIFα (VHL) cKO mice does not perturb normal myelin gene expression and myelination. Previous genetic studies suggest that *Cnp-Cre* elicits gene disruption primarily in the later stages of oligodendrocyte development . For example, disrupting DNA methyltransferase 1 (DNMT1) by *Cnp-Cre* line shows no phenotypes in OPC proliferation and expansion, in sharp contrast to DMNT1 disruption by *Olig1-Cre* which targets the progenitor stages of the oligodendroglial lineage (Moyon et al., 2016). Our recent studies also demonstrated that disrupting Sox2 by *Cnp-Cre* shows no phenotypes in OPC proliferation and expansion, in sharp

contrast to Sox2 disruption by *Sox10-Cre* or *Pdgfrα-CreER*^{T2} which targets OPCs (Zhang et al., 2018a; Zhang et al., 2018b). Therefore, the discrepant phenotypes in HIFα (or VHL) deletion driven by Cnp-Cre versus *Sox10-Cre* or *Pdgfrα-CreER*^{T2} (**Fig. 2, 4, 5**) support the interpretation that HIFα play a major role in OPC differentiation into OLs and is dispensable for oligodendrocyte maturation. Our findings suggest that HIFα signaling pathway regulates postnatal oligodendrocyte development in a stage-dependent manner.

HIFα function is tightly regulated during normal developmental myelination in the early postnatal CNS

We observed inhibition of OPC differentiation in HIFα loss-of-function and gain-of-function. These “contradictory” findings suggest a working model in which endogenous HIFα has to be tightly controlled at an appropriate level for OPC differentiation into OLs. In this regard, HIFα dysregulation (either disruption or hyperactivation) disturbs the timing of OPC differentiation, which is supported by the decreased number of differentiated OLs and unaltered number of OPCs in OPC-specific HIFα loss- and gain-of-function mutants (**Fig. 2B, Fig. 5D**). It remains elusive what factors control the level of endogenous HIFα during developmental myelination. The maturation state of the CNS vasculature, which is responsible for delivering oxygen and nutrients to the parenchymal neural cells, may be a key determinant for HIFα stabilization or degradation. Previous data show that the CNS vasculature is still in immature state and that the white matter angiogenesis, the exclusive avenue of CNS blood vessel formation, actively occurs during early postnatal CNS development (Harb et al., 2013; Yuen et al., 2014). Our immunohistochemical data demonstrate that HIFα is transiently stabilized in the white matter of the spinal cord and the forebrain in the perinatal and early postnatal CNS, presumably reflecting insufficient oxygenation during this time window. The delay of OPC differentiation and myelination in PDGFRα:HIFα cKO mice (**Fig. 2D-E**) is consistent with the

transient HIFα stabilization in the perinatal and early postnatal CNS when white matter angiogenesis is still active .

A paradigm-shift in our mechanistic understanding of HIFα-regulated OPC differentiation

Previous study employed cerebellar slice/cell culture as a studying model and proposed that the “autocrine” activation of Wnt/β-catenin signaling by Wnt7a/Wnt7b plays a crucial role in HIFα stabilization-induced hypomyelination (Yuen et al., 2014). Our data derived from in vivo genetic models do not support this concept. Firstly, unbiased RNA-seq analysis did not reveal dysregulation of the Wnt/β-catenin signaling activity and Wnt7a/Wnt7b expression. Secondly, neither the activity of Wnt/β-catenin signaling nor the expression of Wnt7a/Wnt7b is perturbed in HIFα-stabilized OPCs. Thirdly, disrupting the Wnt secretion mediator WLS blocks OPC-derived autocrine Wnt/β-catenin signaling, but it does not affect the degree of inhibited OPC differentiation and hypomyelination elicited by HIFα hyperactivation. Our findings indicate that Wnt7a/Wnt7b or Wnt/β-catenin signaling is unlikely a direct target of HIFα in the oligodendroglial lineage cells (**Fig. 12N**). The reasons for the different observations between our current study and prior study (Yuen et al., 2014) are unclear. It is possible that cellular non-specificity and/or off-target of pharmacological compounds may underlie the discrepancy. HIFα stabilization induced by hypoxia treatment or by pharmacological DMOG application occurs not only in oligodendroglial lineage cells but also in other lineages of neural cells or vascular cells. Similarly, Wnt/β-catenin inhibition in cultured slices by pharmacological XAV939 or IWP2 treatment also happens in other lineage cells (Yuen et al., 2014). We used cell-specific *Cre-loxP* genetic approaches to circumvent the potential caveats of pharmacological application and convincingly demonstrated that OPC-derived autocrine Wnt/β-catenin plays a minor, if any, role in mediating HIFα-regulated OPC differentiation and myelination.

Another novel finding of this study is the identification of Sox9 as a potential target that mediates HIFα stabilization-elicited inhibition of OPC differentiation (**Fig. 12N,** right panel). Sox9

is highly expressed in neural stem cells (NSCs) (Scott et al., 2010), downregulated in OPCs (Stolt et al., 2003), and completely absent from differentiated OLs (Sun et al., 2017). Sox9 disruption affects OPC specification but not OPC terminal differentiation (Finzsch et al., 2008; Stolt et al., 2003). Recent study suggests that sustained Sox9 expression in OPCs may perturb their normal differentiation (Reiprich et al., 2017). We found that HIFα stabilization activated Sox9 expression in OPCs both *in vitro* and *in vivo*, which is in agreement with previous data showing that Sox9 is transcriptionally activated by HIFα in chondrocytes (Amarilio et al., 2007) and pancreatic β-cell precursor cells (Puri et al., 2013). We found that elevated Sox9 expression perturbed OPC differentiation and that Sox9 knockdown rescued the extent of inhibited OPC differentiation elicited by pharmacological HIFα stabilization in primary OPC culture system. Thus, our study revealed a previously unappreciated HIFα-Sox9 regulation in controlling OPC differentiation.

It should be pointed out that the non-regulation of HIFα-Wnt axis does not negate the crucial role of Wnt/β-catenin in oligodendroglial lineage cells. Previous studies have revealed an inhibitory effect of Wnt/β-catenin activation on OPC differentiation (Guo et al., 2015). However, these studies modulated the signaling activity through manipulating the intracellular components or relevant regulatory molecules within OPCs (Guo et al., 2015), for instance, by disrupting intracellular β-catenin (Fancy et al., 2009; Feigenson et al., 2009; Ye et al., 2009), Axin2 (Fancy et al., 2011), APC (Fancy et al., 2014; Lang et al., 2013), APCDD1 (Lee et al., 2015b), and Daam2 (Lee et al., 2015a). The Wnt-producing cells, which play a crucial role in activating the intracellular Wnt/β-catenin signaling axis in OPCs remain unknown (Guo et al., 2015). Our WLS cKO data demonstrate that oligodendroglial lineage-derived autocrine Wnt plays a minor role in OPC differentiation and myelination in the early postnatal CNS under physiological (**Fig. 10**) or HIFα-stabilized (**Figs. 8, 9**) conditions, suggesting that Wnt ligands derived from other lineage cells may be responsible for control OPC differentiation through paracrine Wnt signaling. Previous RNA-seq data (Zhang et al., 2014) indicate that astrocytes may be the major cellular

source of Wnt proteins, for example Wnt7a, which had been shown inhibiting OPC differentiation through activating canonical Wnt signaling in OPCs (Yuen et al., 2014). Future studies are needed to test the tempting hypothesis that astrocyte-derived paracrine Wnt signaling may play major a role in controlling OPC differentiation under normal or HIFα-stabilized conditions.

Implication of our findings in neonatal white matter injury (WMI)

Disturbance of normal developmental myelination (hypomyelination) is one of the established pathological hallmarks in preterm (or premature) infants born before 37th week gestational ages with very low birth weight (Back, 2017; Deng, 2010). Hypoxia/ischemia-induced diffuse WMI frequently occurs in preterm infants due to the anatomical and physiological immaturity of the respiratory system and the brain white matter vasculature. We demonstrated that, compared with healthy controls, HIF1α was markedly upregulated in the brain white matter of mice subjected to neonatal hypoxia-ischemia injury (**Fig. 1E**). Our findings that HIFα hyperactivity disturbs OPC differentiation and results in hypomyelination suggest that oligodendroglial HIFα upregulation may play a crucial role in hypoxia-ischemia-induced myelination disturbance. The function and molecular mechanisms of oligodendroglial HIFα in hypoxia-ischemia-induced hypomyelination (Liu et al., 2011) have not been defined in genetic animal models. Our *in vivo* data indicate that HIFα stabilization in response to hypoxia-ischemia injury may inhibit OPC differentiation and cause hypomyelination and that the underlying mechanisms may be independent of the autocrine canonical Wnt signaling. In the future, we plan to use the cell-specific genetic models (HIFα loss and gain-of-function) generated in the current study to test this hypothesis.

Figures and Legends

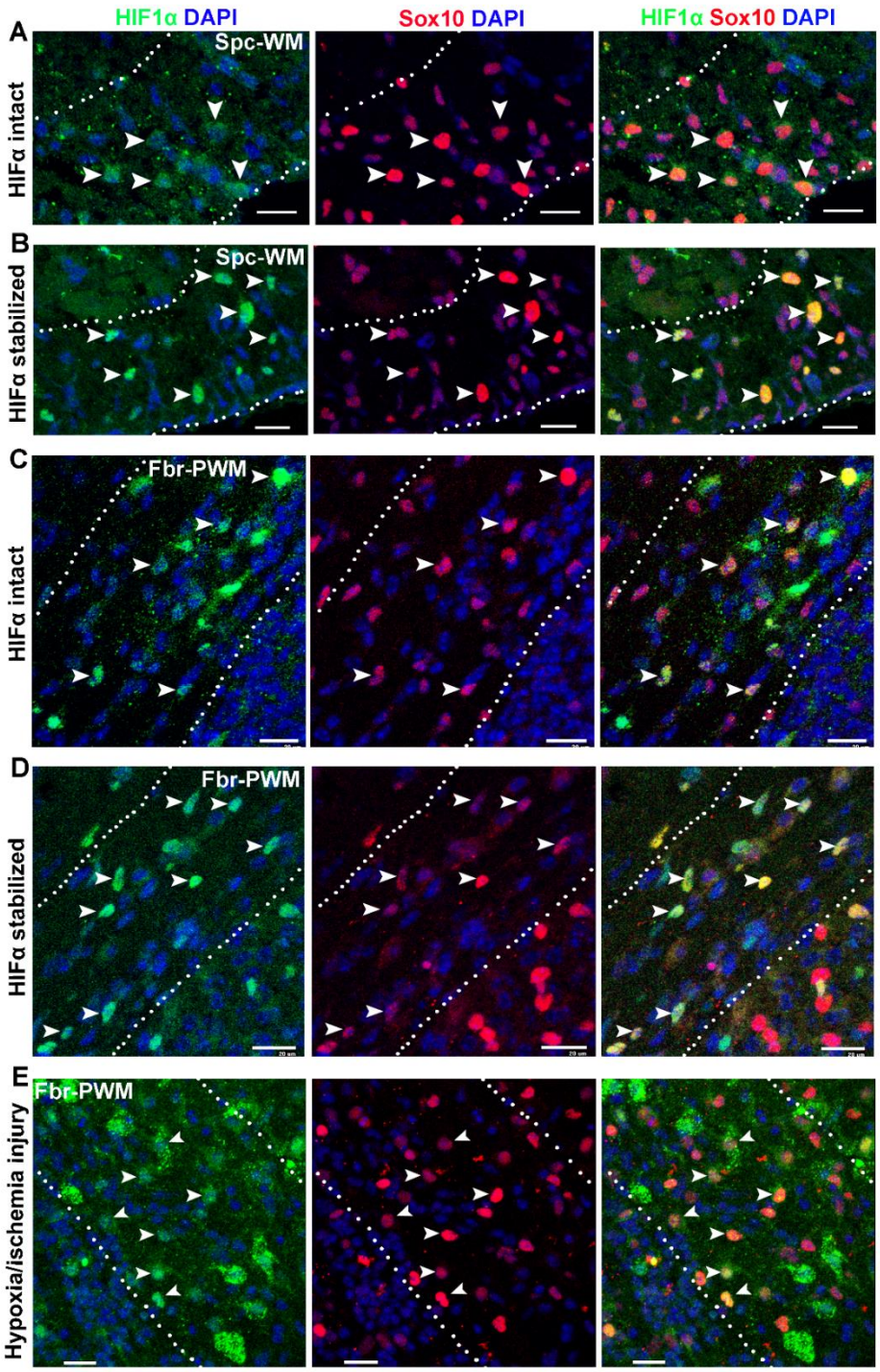

Figure 1 – HIFα stabilization in the early postnatal murine CNS. **A-B**, immunohistochemistry (IHC) of HIF1α and oligodendroglial lineage marker Sox10 in the spinal cord ventral white matter (Spc-WM, marked by dotted lines) of HIFα intact mice (**A**) and HIFα stabilized (*Sox10-*

Cre:Vhl$^{fl/fl}$) mice (**B**) at postnatal day 5 (P5). **C-D**, IHC of HIF1α and Sox10 in the forebrain periventricular white matter (Fbr-PWM, marked by dotted lines) of HIFα intact mice (**C**) and HIFα stabilized (*Sox10-Cre:Vhl*$^{fl/fl}$) mice (**D**) at P5. **E**, IHC of HIF1α and Sox10 in the Fbr-PWM of P10 HIFα intact mice that had been subjected to hypoxia/ischemia injury on P6 (see Materials and Methods for details). Arrowheads in **A-E** point to HIF1α$^+$Sox10$^+$ cells. Scale bars, 20 µm.

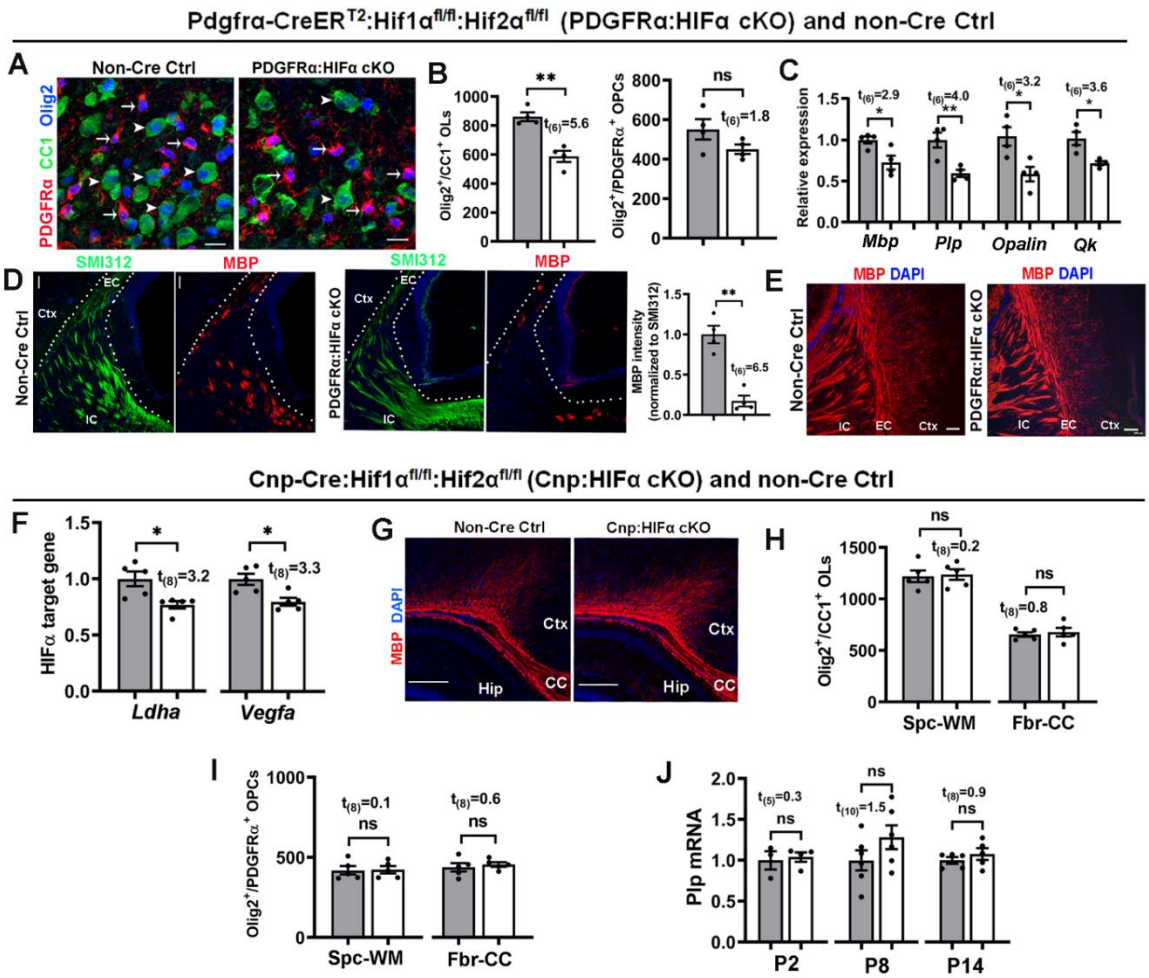

Figure 2 – Oligodendroglial HIFα regulates myelination by controlling upstream OPC differentiation but not downstream OL lineage maturation. A-E, PDGFRα:HIFα cKO and non-Cre littermate control mice were treated with tamoxifen at P1, P2, and P3, and analyzed at P8 (n=4 each group) and P14 (n=3 each group). **A-B**, IHC (**A**) and quantification (**B**) of Olig2$^+$CC1$^+$ OLs and Olig2$^+$PDGFRα$^+$ OPCs in the spinal cord. **C**, relative expression of myelin

protein genes of myelin basic protein (*Mbp)* and proteolipid protein (*Plp)* and mature OL-specific gene of *Opalin* and quake (*Qk,* aka CC1*)* in the forebrain measured by real-time quantitative PCR (RT-qPCR). **D**, IHC of myelin marker MBP and pan-axonal marker SMI312 in forebrain periventricular white matter (left, marked by dotted area) and quantification (right) at P8. EC, external capsule, IC, internal capsule, Ctx, cortex. **E**, IHC of MBP in forebrain periventricular white matter at P14 (tamoxifen at P1, P2, and P3). **F-J**, Cnp:HIFα cKO and non-Cre littermate control mice were analyzed at P2, P8, and P14. **F**, RT-qPCR quantification of HIFα target genes Ldha and Vegfa in P8 spinal cord. **G**, myelin staining by MBP in the forebrain. CC, corpus callosum, Ctx, cortex, Hip, hippocampus. **H-I**, densities (#/mm^2) of Olig2$^+$CC1$^+$ OLs (**H**) and Olig2$^+$PDGFRα$^+$ OPCs (**I**) at P14. Spc-WM: spinal cord white matter, Fbr-CC: forebrain corpus callosum. **J**, RT-qPCR assay of exon3b-containing Plp mRNA, which is specific to mature OLs, in the spinal cord at different time points. Data are presented as mean ± s.e.m.; gray bars are from control, white bars cKO; * $P<0.05$, ** $P<0.01$, *** $P<0.001$, ns, not significant $P>0.05$. The above data presentation and statistics are applied to all figures except indicated otherwise). Scale bar, A, 10um, D, 20um, E, 100um, G, 250um

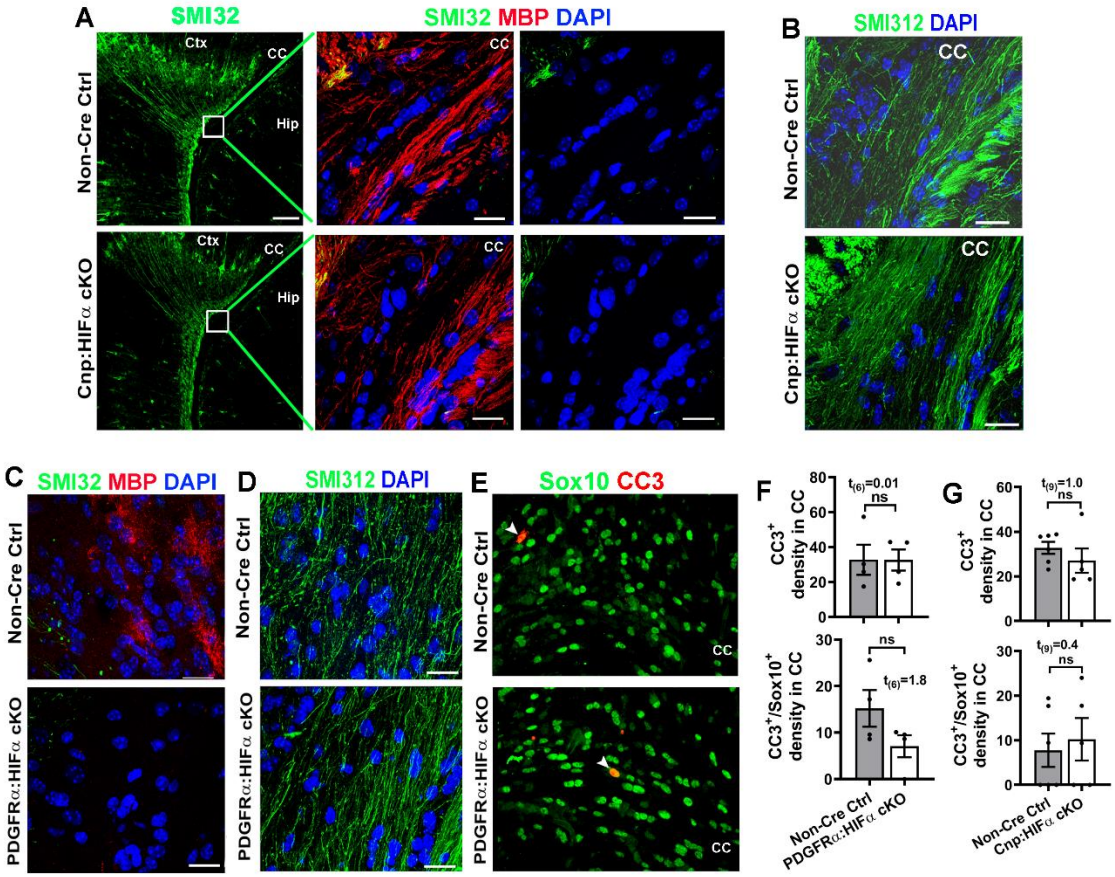

Figure 3 – Oligodendroglial HIFα is dispensable for axonal integrity or cell death. **A**, immunostaining images of P14 forebrain using SMI32, a monoclonal antibody recognizing the non-phosphorylated neurofilament proteins of heavy chain (NFH), which has been reported expressing in injured axons and in a subset of pyramidal neuron bodies and dendrites. Boxed areas show the corpus callosum (CC) at higher magnification images of SMI32 and MBP in the right panels. Ctx, cortex, Hip, hippocampus. Note the absence of SMI32-positive signals in the CC of both non-Cre Ctrl and Cnp:HIFα cKO mice. **B**, immunostaining images of P14 CC using SMI312, a monoclonal antibody recognizing both phosphorylated and non-phosphorylated NFH (a pan-axonal marker). **C-D**, IHC of SMI32/MBP (**C**) and SMI312 (**D**) in the CC of P8 non-Cre Ctrl and PDGFRα:HIFα cKO mice (tamoxifen injection at P1, P2, and P3). **E-F**, representative confocal images and quantification of cells positive for cleaved caspase 3 (CC3) and/or pan-

oligodendroglial lineage marker Sox10 in P8 CC of PDGFRα:HIFα cKO and control mice. Arrowheads point to $CC3^+/Sox10^+$ cells. **G**, quantification of $CC3^+$ and $CC3^+/Sox10^+$ cells in P14 CC of Cnp:HIFα cKO and control mice. Scale bar, A, 100µm (low magnification), 20µm (high magnification); B-E, 20µm.

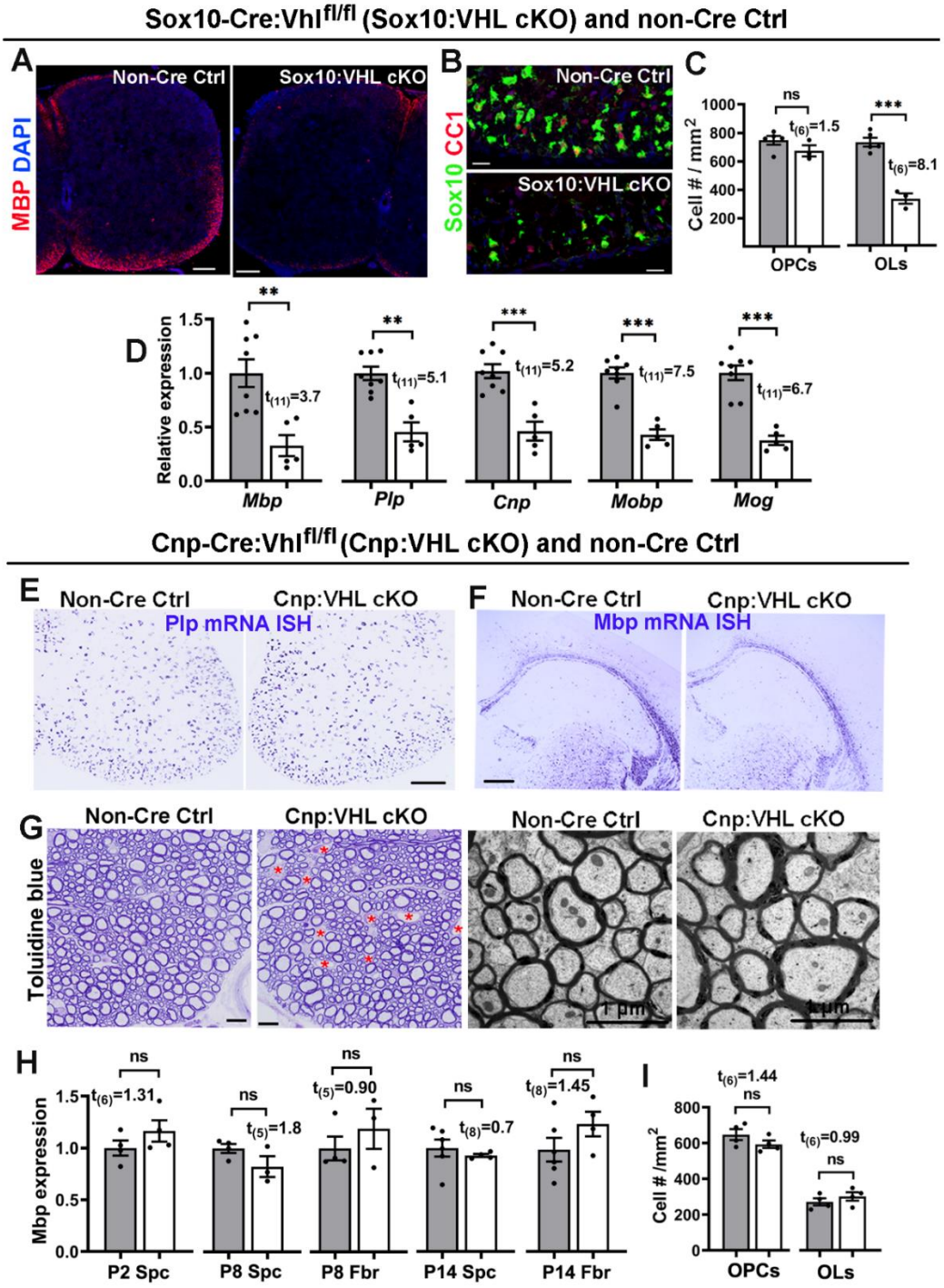

Figure 4 – HIFα stabilization impairs myelination by inhibiting upstream OPC differentiation but not downstream OL lineage maturation. A, Myelin staining of MBP in the spinal cord of *Sox10-Cre:Vhl*$^{fl/fl}$ (Sox10:VHL cKO) and non-Cre control littermates at P5. Most

Sox10:VHL cKO pups died by the first postnatal week. **B**, representative confocal images of Sox10 and differentiated OL marker CC1 in P5 spinal cord (n=5 Ctrl, 3 cKO). **C**, quantification of Sox10$^+$CC1$^+$ OLs and Sox10$^+$PDGFRa$^+$ OPCs (right) in P5 spinal cord (n=8 Ctrl, 5 cKO). **D**, RT-qPCR assay of myelin-specific genes in the spina cord at P5. *Cnp*, 2',3'-Cyclic-nucleotide 3'-phosphodiesterase; *Mobp*, myelin oligodendrocyte basic protein; *Mog*, myelin oligodendrocyte glycoprotein. **E-F**, mRNA in situ hybridization (ISH) of *Plp* and *Mbp* in the spina cord (**E**) and forebrain (**F**) of *Cnp-Cre:Vhl*$^{fl/fl}$ (Cnp:VHL cKO) and Non-Cre Ctrl littermates at P14. **G**, myelination in the adult spinal cord indicated by toluidine blue staining of semithin sections (left) and transmission electron microscopy of ultrathin section (right). Red asterisks in **G** denotes blood vessels, the density of which is elevated in Cnp:VHL cKO mice (Guo et al., 2015). **H**, *Mbp* mRNA levels quantified by RT-qPCR in Cnp:VHL cKO and non-Cre Ctrl mice at different time points. Spc, spinal cord; Fbr, forebrain. **I**, densities of Sox10$^+$CC1$^+$ OLs and Sox10$^+$PDGFRα$^+$ OPCs in P8 spinal cord of Cnp:VHL cKO and non-Cre Ctrl mice. Scale bars: A, 100µm, B, 20µm, E-F, 200µm, G, 10µm (left), 1µm (right).

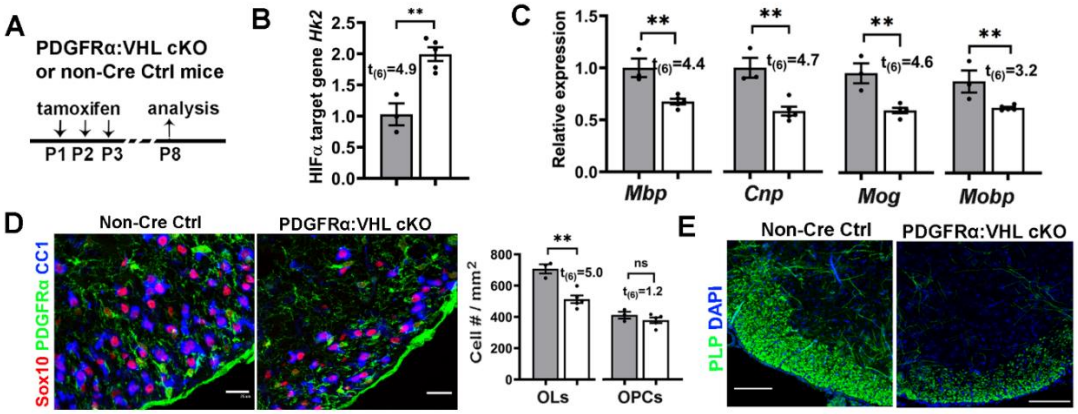

Figure 5 – Inducible HIFα stabilization in postnatal OPCs inhibits OPC differentiation. A, experimental design for B-E. PDGFRα:VHL cKO (*Pdgfrα-CreER*^{T2}:*Vhl*$^{fl/fl}$ n=5) and non-Cre Ctrl (n=3) mice were treated with tamoxifen intraperitoneally at P1, P2, and P3, and analyzed at P8. **B**, RT-qPCR quantification of HIFα target gene hexokinase 2 *Hk2* in the spinal cord. **C**,

expression of major myelin proteins in the spinal cord quantified by RT-qPCR. **D**, representative confocal images and the density of Sox10^{+}/CC1^{+} OLs and Sox10^{+}/PDGFRα^{+} OPCs. **E**, IHC of PLP showing myelination in the spinal cord ventral white matter. Scale bars, D, 25µm, E, 100µm.

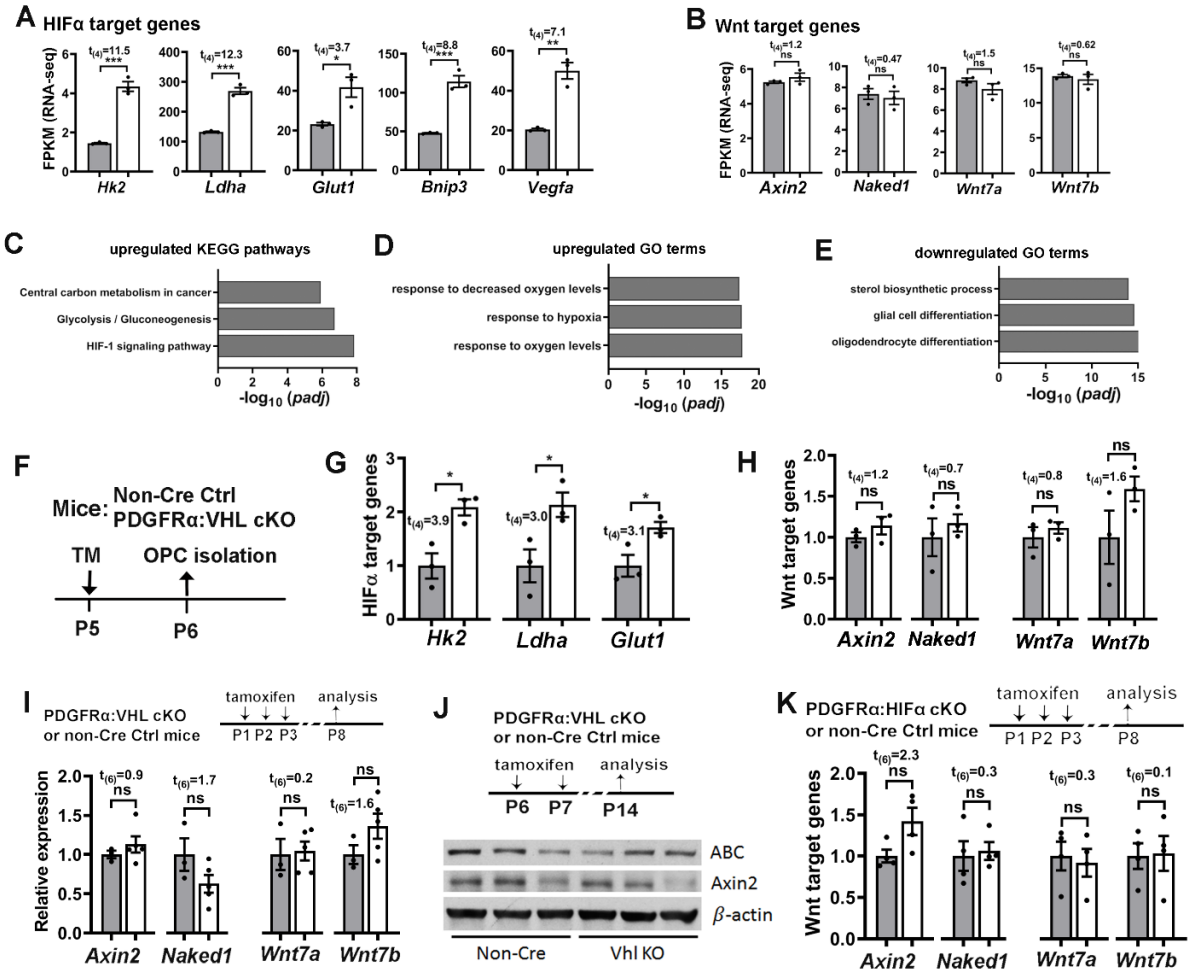

Figure 6 – **Stabilizing HIFα activates HIFα-mediated signaling, but does not perturb Wnt/β-catenin signaling in the oligodendroglial lineage and in the CNS. A-B,** relative expression of HIFα and Wnt target genes from unbiased RNA-seq analysis. FPKM, fragments per kilobase of transcript per million mapped reads, a normalized measurement of gene expression. The RNA was prepared from the spinal cord of P5 *Sox10-Cre:Vhl*$^{fl/fl}$ mice (n=3,

white bars) and non-Cre littermate controls (n=3, gray bars). **C-E**, Top 3 significant enriched KEGG pathway and gene ontology (GO) terms among 255 upregulated and 351 downregulated genes derived from unbiased RNA-seq. Note that HIFα signaling pathway (**C**) and response to hypoxia (**D**) were significantly upregulated, validating HIFα hyperactivation in *Sox10-Cre:Vhl*$^{fl/fl}$ mice and that oligodendroglial cell differentiation was significantly downregulated (**E**), which is agreement with the data of **Fig. 4A-D**. **F**, experimental design for **G** and **H**. PDGFRα:VHL cKO (n=3, white bars) and non-Cre control littermates (n=3, gray bars) were treated with tamoxifen (TM) at P5, and forebrain OPCs at P6 were acutely purified by MACS. **G**-**H**, RT-qPCR quantification of HIFα target gene (**G**) and Wnt target gene (**H**) expression in purified OPCs. **I**, expression of Wnt target gene (*Axin2* and *Naked1*) and *Wnt7a/7b* in P8 spinal cord (n=3 Ctrl, gray bars, 5 PDGFRα cKO, white bars) quantified by RT-qPCR. **J**, Western blot assay of the active form of β-catenin (ABC) and Axin2 in P14 forebrain (n=3 each group). **K**, expression of Wnt target genes (*Axin2* and *Naked1*) and *Wnt7a/7b* in P8 spinal cord measured by RT-qPCR (n=4 each group).

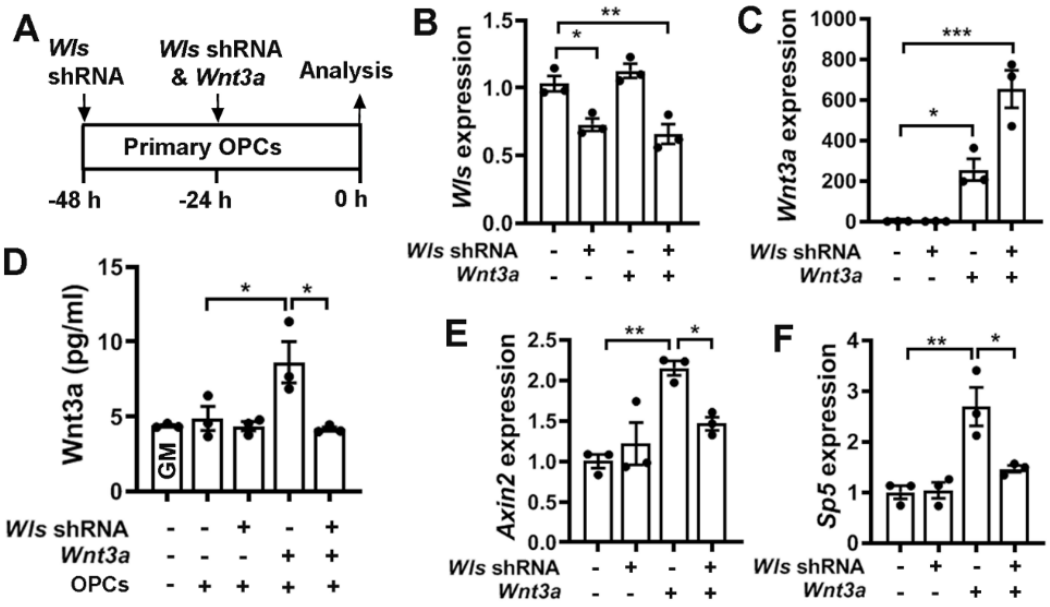

Figure 7- WLS deficiency inhibits Wnt3a secretion and blocks autocrine Wnt/β-catenin signaling activity in OPCs. A, experimental design of cell transfection of Wls shRNA and Wnt3a-expressing plasmids to forebrain primary OPC cultured in the growth medium. **B-C**, RT-qPCR assay of *Wls* (**B**) and *Wnt3a* (**C**) expression in transfected primary OPCs. One-way ANOVA followed by Tukey's multiple comparisons, $F_{(3, 8)} = 15.39$, $P = 0.001$ *Wls*, $F_{(3, 8)} = 32.81$, $P < 0.0001$ *Wnt3a*. **D**, ELISA quantification of Wnt3a in the growth medium (GM) in the absence or presence of OPCs transfected by Wls shRNA and/or Wnt3a. One-way ANOVA followed by Tukey's multiple comparisons, *** $P < 0.001$, ns not significant. $F_{(4, 10)} = 6.70$, $P < 0.0069$. Note that Wnt3a concentration in the GM in the presence of primary OPCs is statistically indistinguishable from that in the GM alone, suggesting that intact primary OPCs do not secrete Wnt3a. **E-F**, RT-qPCR quantification of Wnt target genes *Axin2* and *Sp5* in OPCs transfected with Wls shRNA and/or Wnt3a. One-way ANOVA followed by Tukey's multiple comparisons, $F_{(3, 8)} = 11.06$, $P = 0.0032$ *Axin2*, $F_{(3, 8)} = 13.25$, $P = 0.0018$ *Sp5*.

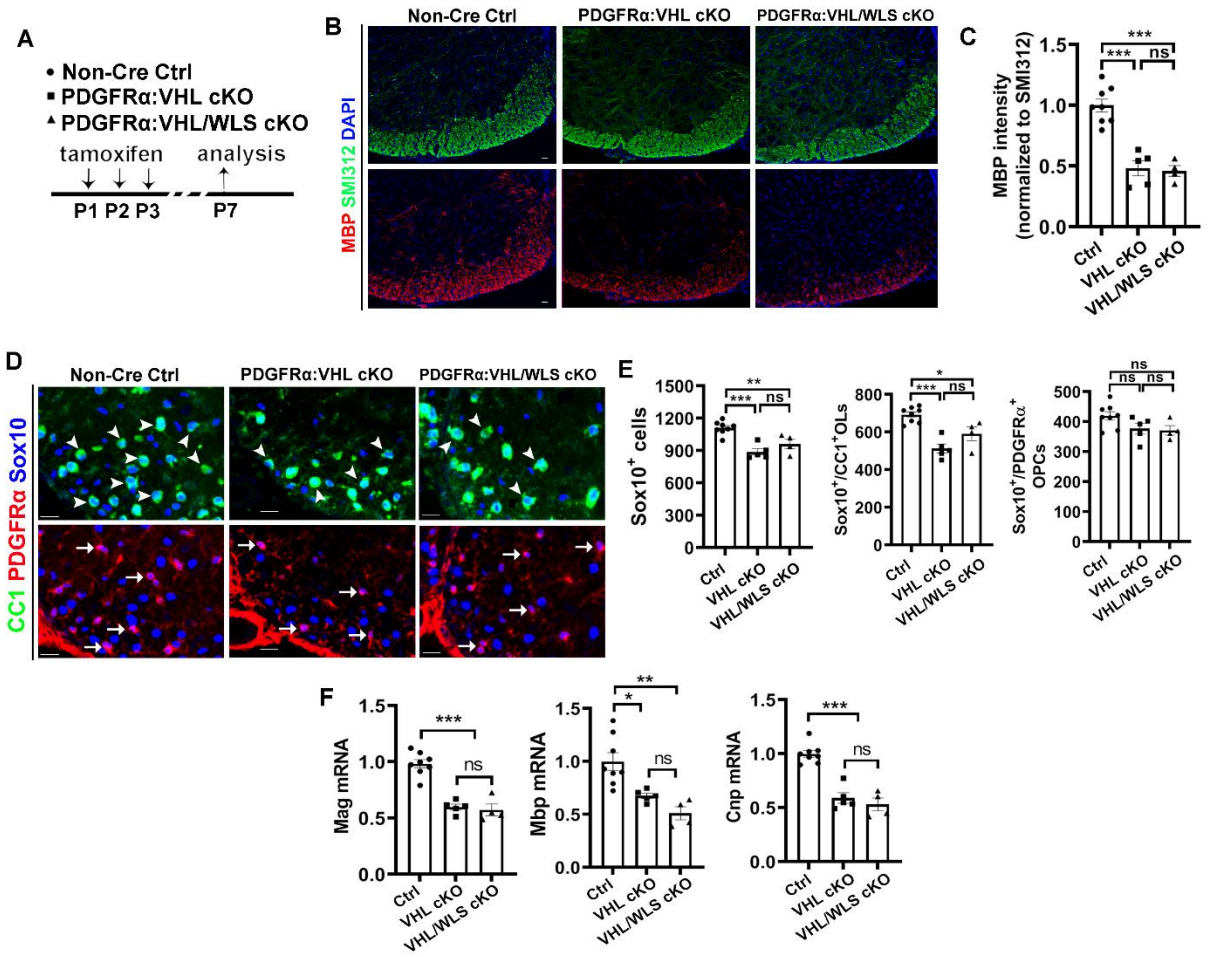

Figure 8 – Disrupting WLS in PDGFRα-expressing OPCs does not affect the degree of inhibited OPC differentiation and hypomyelination elicited by HIFα hyperactivation. **A**, experimental design for **B-F**. PDGFRα:VHL cKO, *Pdgfrα-CreER*^{T2}:*Vhl*$^{fl/fl}$ (n=5); PDGFRα:VHL/WLS cKO, *Pdgfrα-CreER*^{T2}:*Vhl*$^{fl/fl}$:Wls$^{fl/fl}$ (n=4); Non-Cre Ctrl, *Vhl*$^{fl/fl}$ and/or Wls$^{fl/fl}$ (n=8). **B-C**, representative confocal images (**B**) and quantification (**C**) of myelination by MBP staining. The signal of SMI312, pan-axonal marker is indistinguishable among each group and used as an internal control of MBP quantification. One-way ANOVA followed by Tukey's multiple comparisons, $F_{(2, 14)}$=31.93 P < 0.0001. **D-E**, representative confocal images (**D**) and quantification (**E**) of Sox10$^+$/CC1$^+$ differentiated OLs (**D**, arrowheads), Sox10$^+$/PDGFRα$^+$ OPCs (**D**, arrows), and Sox10$^+$ oligodendroglial lineage cells in the spinal cord. One-way ANOVA

followed by Tukey's multiple comparisons, $F_{(2, 14)} = 17.34$ $P = 0.0002$ Sox10$^+$, $F_{(2, 14)} = 18.44$ $P = 0.0001$ Sox10$^+$/CC1$^+$, $F_{(2, 14)} = 2.967$ $P = 0.0843$ Sox10$^+$/PDGFRα$^+$. **F**, RT-qPCR quantification of mature OL-enriched genes in the spinal cord. One-way ANOVA followed by Tukey's multiple comparisons, $F_{(2, 14)} = 11.53$ $P = 0.0011$ *Mbp*, $F_{(2, 14)} = 39.88$ $P < 0.0001$ *Mag*, $F_{(2, 14)} = 38.78$ $P < 0.0001$ *Cnp*. Scale bars=20µm.

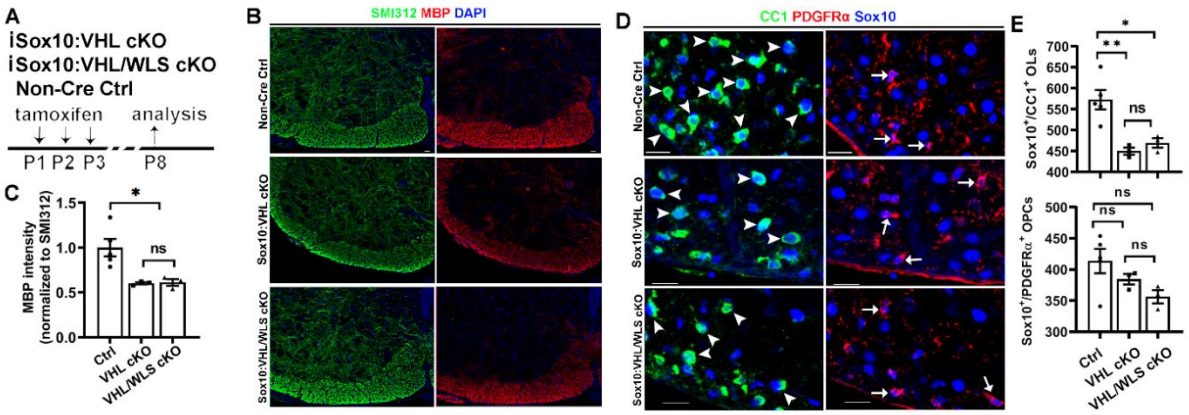

Figure 9 - Disrupting WLS in Sox10-expressing oligodendroglial lineage cells does not affect HIFα hyperactivation-elicited inhibition of OPC differentiation and hypomyelination. **A**, experimental design for **B-E**. tamoxifen inducible *Sox10-CreER*^{T2}:*Vhl*$^{fl/fl}$ (iSox10:VHL cKO n=3); *Sox10-CreER*^{T2}:*Vhl*$^{fl/fl}$:Wls$^{fl/fl}$ (iSox10:VHL/WLS cKO, n=3); *Vhl*$^{fl/fl}$ and/or Wls$^{fl/fl}$ (Non-Cre Ctrl, n=5). **B-C**, representative confocal images (**B**) and quantification (**C**) of myelination by MBP staining of the spinal cord. SMI312 signal was used as an internal control of MBP quantification. One-way ANOVA followed by Tukey's multiple comparisons, $F_{(2, 8)}= 8.484$ $P = 0.0105$. **D-E**, representative confocal images (**D**) and quantification (**E**) of Sox10$^+$/CC1$^+$ differentiated OLs (**D**, arrowheads) and Sox10$^+$/PDGFRα$^+$ OPCs (**D**, arrows) in the spinal cord. One-way ANOVA followed by Tukey's multiple comparisons, $F_{(2, 8)} = 11.90$ $P = 0.004$ Sox10$^+$/CC1$^+$, $F_{(2, 14)} = 2.880$ $P = 0.1143$ Sox10$^+$/PDGFRα$^+$. Scale bars=20µm.

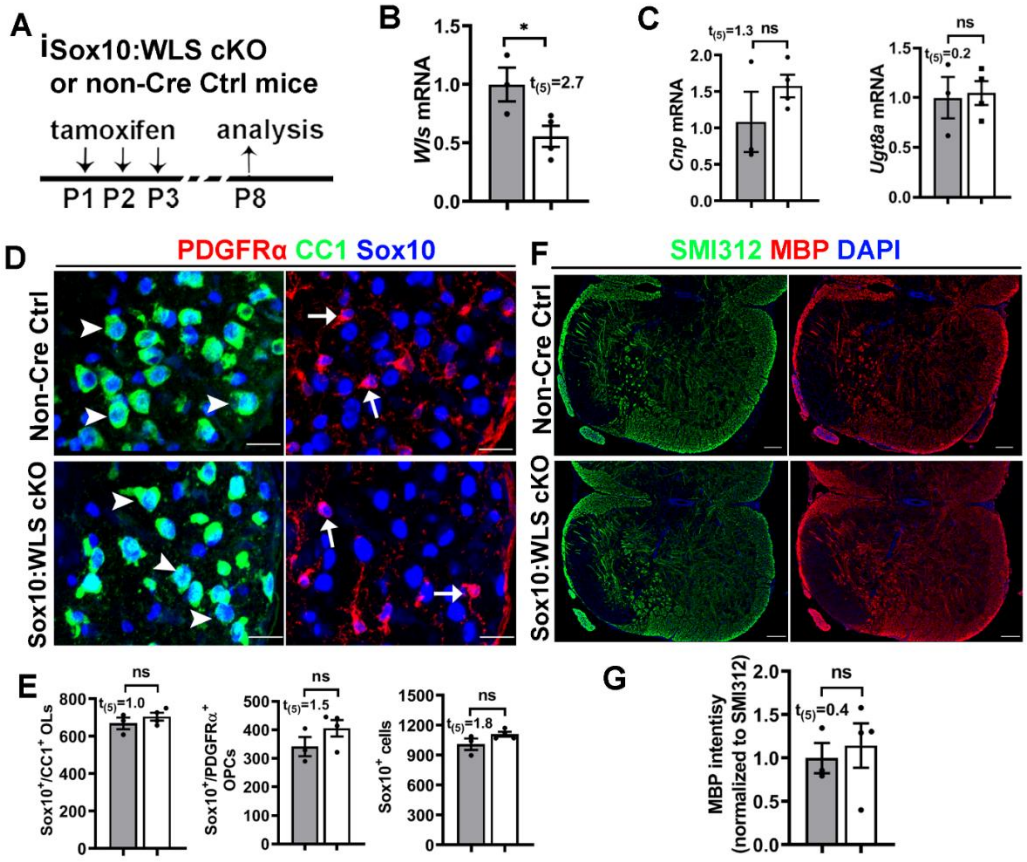

Figure 10 – Disrupting WLS in Sox10-expressing oligodendroglial lineage cells does not perturb normal OPC differentiation and myelination. A, experimental design for **B-G**. Tamoxifen inducible *Sox10-CreER*^{T2}:*Wls*$^{fl/fl}$ (iSox10:WLS cKO, n=4); Wls$^{fl/fl}$ (non-Cre Ctrl, n=3). **B-C**, RT-qPCR quantification of Wls (**B**) and differentiated OL-enriched gene Cnp and Ugt8a (**C**) in the spinal cord. **D-E**, representative confocal images (**D**) and quantification (**E**) of Sox10^{+}/CC1^{+} differentiated OLs (**D**, arrowheads), Sox10^{+}/PDGFRα^{+} OPCs (**D**, arrows), and Sox10^{+} oligodendroglial lineage cells in the spinal cord. **F-G**, representative confocal images (**B**) and quantification (**C**) of myelination by MBP staining of the spinal cord. SMI312 signal was used as an internal control of MBP quantification. Scale bars, D, 20µm, E, 50µm.

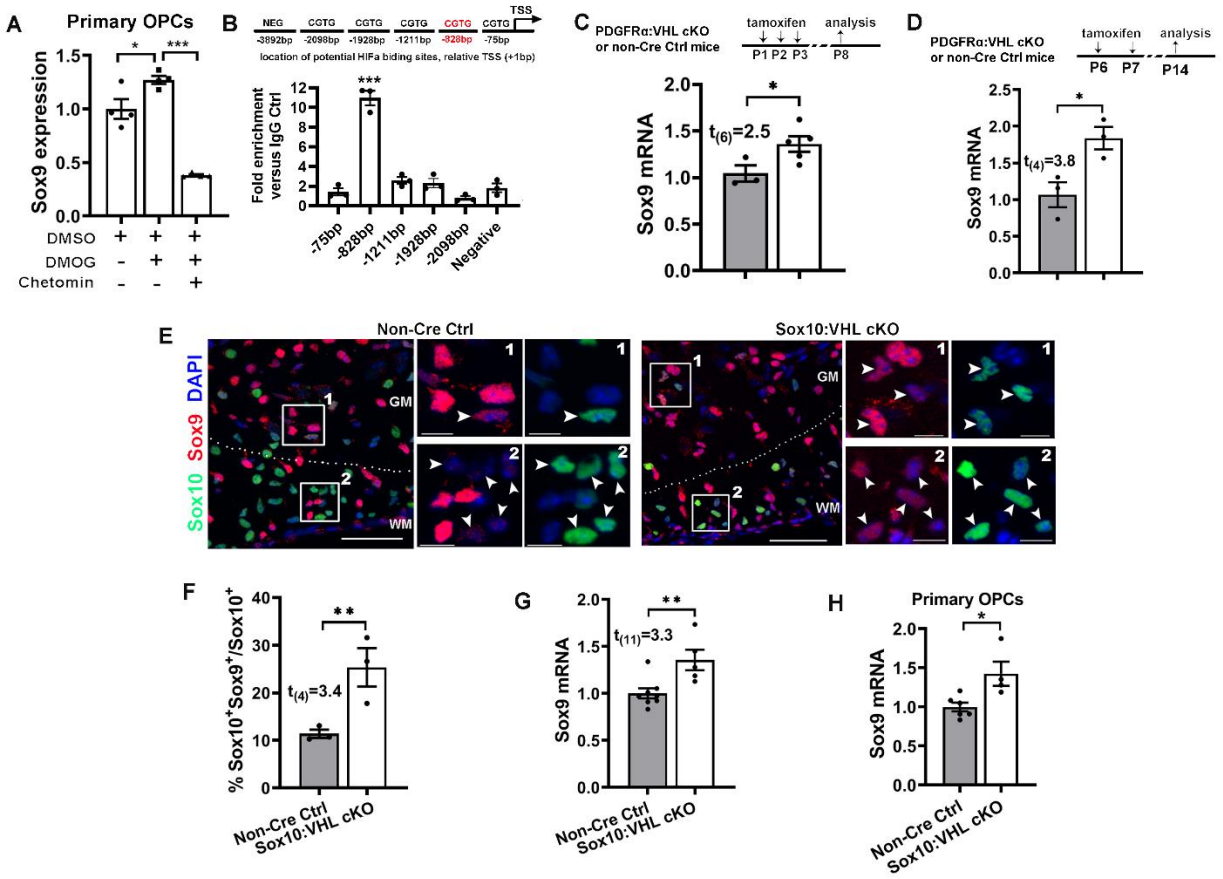

Figure 11 – HIFα stabilization activates Sox9 expression. A, Sox9 expression in the purified primary OPCs assessed by RT-qPCR. Purified cortical OPCs from neonatal rat brains were treated with HIFα stabilizer dimethyloxalylglycine (DMOG, 1mM) in the absence and presence of HIFα signaling blocker chetomin (100nM) for 7 h. n=4 each group. One-way ANOVA followed by Tukey's multiple comparisons, $F_{(2, 9)} = 62.53$ $P < 0.0001$. **B**, potential HIFα binding sites (CGTG) in the upstream sequence of rat Sox9 genes (+1bp is defined as the transcription start site, TSS) and ChIP-qPCR verification of physical binding of HIFα to the promoter region of -828bp in primary OPCs treated with DMOG. One way ANOVA with Dunnete test comparing each group with negative control. $F_{(2,12)} = 69.21$ $P < 0.0001$. **C**, RT-qPCR quantification of Sox9 expression in P8 spinal cord of PDGFRα:VHL cKO (n=5) and non-Cre control (n=3) mice that had been treated with tamoxifen at P1, P2, and P3. **D**, RT-qPCR quantification of Sox9

expression in P14 spinal cord of PDGFRα:VHL cKO (n=3) and non-Cre control (n=3) mice that had received tamoxifen at P6 and P7. **E**, confocal images showing that Sox9 is barely expressed in Sox10^{+} oligodendroglial lineage cells in the spinal cord of non-Cre control but upregulated in Sox10:VHL cKO mice at P5. WM, white matter, GM, gray matter. The boxed areas of #1 and #2 were shown at higher magnification at the right. **F**, percentage of Sox10^{+} oligodendroglial lineage cells expressing Sox9 in the spinal cord (n=3 each group). **G**, RT-qPCR quantification of Sox9 mRNA in the spinal cord of non-Cre control (n=8) and Sox10:VHL cKO (n=5) mice at P5. **H**, RT-qPCR assay of Sox9 expression in primary OPCs isolated from the neonatal brain of *Sox10-Cre:Vhl*$^{fl/fl}$ (n=4) and non-Cre control (n=6) pups. Scale bars, 50μm in D and 10 μm in boxed areas of panel E.

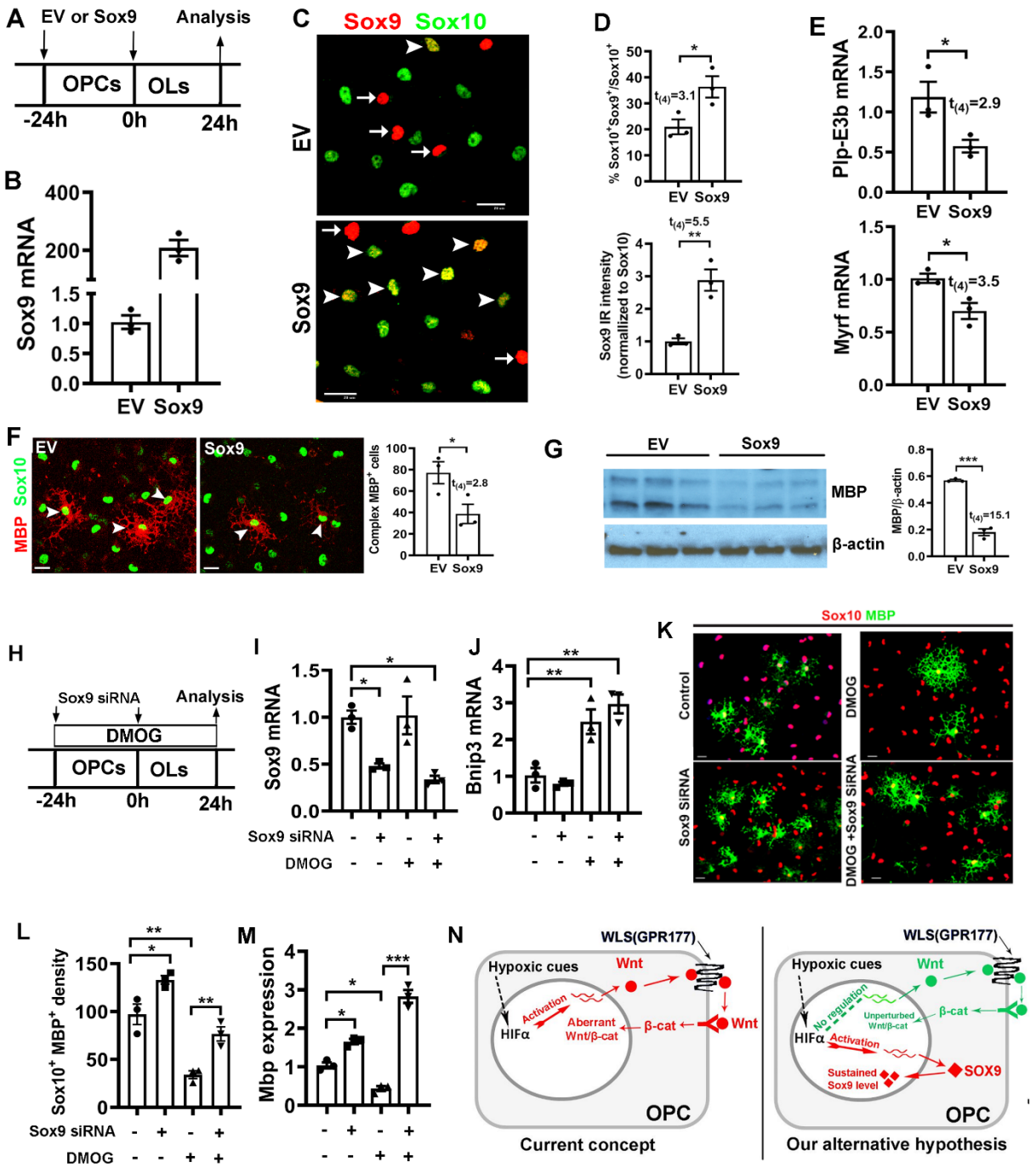

Figure 12 – Sustained Sox9 expression inhibits OPC differentiation. **A**, experimental design for **B-G**. Cortical primary OPCs in growth medium were transfected with Sox9-expressing plasmid (Sox9, n=3) or empty vector (EV, n=3), then differentiate for 24 h in serum-free differentiating medium. **B**, RT-qPCR quantification of Sox9 mRNA expression. **C,**

representative immunocytochemical images of Sox9/Sox10. Arrowheads point to $Sox9^+/Sox10^+$ oligodendrocytes and arrows point to $Sox9^+/Sox10^-$ cells, which are presumably astrocytes. Scale bar=20μm. **D,** percentage of $Sox10^+$ oligodendroglial lineage cells that express Sox9 (top) and Sox9 immunoreactive intensity normalized to Sox10 (bottom). **E**, RT-qPCR assay of exon3b-containing Plp (Plp-E3b), which specifically expresses in differentiated OLs, and myelin regulatory factor (Myrf), a potent pro-differentiation gene. **F**, representative immunocytochemical images of MBP/Sox10 and density (#/mm^2) of $Sox10^+$ oligodendroglial cells of complex ramified morphology indicated by MBP staining (arrowheads in **F**), Scale bar=10μm. **G**, Western blot images and quantification of MBP and internal loading control β-actin. **H**, experimental designs for panels **I-M**, primary OPCs were treated with HIFα stabilizer DMOG and transfected with Sox9 siRNA twice with 24 h apart. **I-J**, expression of Sox9 (**I**) and HIFα target gene Bnip3 (**J**) quantified by RT-qPCR. One way ANOVA followed by Tukey's test; $F_{(3, 8)} = 10.33$, $P = 0.004$ *Sox9;* $F_{(3, 8)} = 20.83$, $P = 0.0004$ *Bnip3.* **K**, representative immunostaining images of differentiated OLs labeled by MBP and Sox10. Scale bar=10μm. **L-M**, density (#/mm^2) of $MBP^+/Sox10^+$ differentiated OLs (**L**) and RT-qPCR assay of Mbp mRNA expression (**M**). One way ANOVA followed by Tukey's test; $F_{(3, 8)} = 33.29$, $P < 0.0001$ $MBP^+/Sox10^+$*;* $F_{(3, 8)} = 97.96$, $P < 0.0001$ *Mbp.* **N**, previously proposed and our alternative working model explaining the role of HIFα in OPC differentiation. Endogenous HIFα regulates CNS myelination by controlling upstream OPC differentiation but not downstream OL maturation in perinatal and early postnatal CNS whereas aberrant HIFα activation (via VHL mutation of hypoxia-ischemia insult) inhibits OPC differentiation through the Wnt-independent and Sox9-dependent pathway.

Reference

Amarilio, R., S.V. Viukov, A. Sharir, I. Eshkar-Oren, R.S. Johnson, and E. Zelzer. 2007. HIF1alpha regulation of Sox9 is necessary to maintain differentiation of hypoxic prechondrogenic cells during early skeletogenesis. *Development*. 134:3917-3928.

Back, S.A. 2017. White matter injury in the preterm infant: pathology and mechanisms. *Acta Neuropathol*. 134:331-349.

Banziger, C., D. Soldini, C. Schutt, P. Zipperlen, G. Hausmann, and K. Basler. 2006. Wntless, a conserved membrane protein dedicated to the secretion of Wnt proteins from signaling cells. *Cell*. 125:509-522.

Bartscherer, K., N. Pelte, D. Ingelfinger, and M. Boutros. 2006. Secretion of Wnt ligands requires Evi, a conserved transmembrane protein. *Cell*. 125:523-533.

Campbell, M.J., and J.H. Morrison. 1989. Monoclonal antibody to neurofilament protein (SMI-32) labels a subpopulation of pyramidal neurons in the human and monkey neocortex. *J Comp Neurol*. 282:191-205.

Cunningham, L.A., K. Candelario, and L. Li. 2012. Roles for HIF-1alpha in neural stem cell function and the regenerative response to stroke. *Behav Brain Res*. 227:410-417.

Deng, W. 2010. Neurobiology of injury to the developing brain. *Nat Rev Neurol*. 6:328-336.

Emery, B., D. Agalliu, J.D. Cahoy, T.A. Watkins, J.C. Dugas, S.B. Mulinyawe, A. Ibrahim, K.L. Ligon, D.H. Rowitch, and B.A. Barres. 2009. Myelin gene regulatory factor is a critical transcriptional regulator required for CNS myelination. *Cell*. 138:172-185.

Fancy, S.P., S.E. Baranzini, C. Zhao, D.I. Yuk, K.A. Irvine, S. Kaing, N. Sanai, R.J. Franklin, and D.H. Rowitch. 2009. Dysregulation of the Wnt pathway inhibits timely myelination and remyelination in the mammalian CNS. *Genes Dev*. 23:1571-1585.

Fancy, S.P., E.P. Harrington, S.E. Baranzini, J.C. Silbereis, L.R. Shiow, T.J. Yuen, E.J. Huang, S. Lomvardas, and D.H. Rowitch. 2014. Parallel states of pathological Wnt signaling in neonatal brain injury and colon cancer. *Nat Neurosci*.

Fancy, S.P., E.P. Harrington, T.J. Yuen, J.C. Silbereis, C. Zhao, S.E. Baranzini, C.C. Bruce, J.J. Otero, E.J. Huang, R. Nusse, R.J. Franklin, and D.H. Rowitch. 2011. Axin2 as regulatory and therapeutic target in newborn brain injury and remyelination. *Nat Neurosci*. 14:1009-1016.

Feigenson, K., M. Reid, J. See, E.B. Crenshaw, 3rd, and J.B. Grinspan. 2009. Wnt signaling is sufficient to perturb oligodendrocyte maturation. *Mol Cell Neurosci*. 42:255-265.

Finzsch, M., C.C. Stolt, P. Lommes, and M. Wegner. 2008. Sox9 and Sox10 influence survival and migration of oligodendrocyte precursors in the spinal cord by regulating PDGF receptor alpha expression. *Development*. 135:637-646.

Guo, F., J. Lang, J. Sohn, E. Hammond, M. Chang, and D. Pleasure. 2015. Canonical Wnt signaling in the oligodendroglial lineage-puzzles remain. *Glia*.

Harb, R., C. Whiteus, C. Freitas, and J. Grutzendler. 2013. In vivo imaging of cerebral microvascular plasticity from birth to death. *Journal of cerebral blood flow and metabolism : official journal of the International Society of Cerebral Blood Flow and Metabolism*. 33:146-156.

Haynes, R.L., N.S. Borenstein, T.M. Desilva, R.D. Folkerth, L.G. Liu, J.J. Volpe, and H.C. Kinney. 2005. Axonal development in the cerebral white matter of the human fetus and infant. *J Comp Neurol*. 484:156-167.

Huang, H., X.F. Zhao, K. Zheng, and M. Qiu. 2013. Regulation of the timing of oligodendrocyte differentiation: mechanisms and perspectives. *Neuroscience bulletin*. 29:155-164.

Ivanovic, Z. 2009. Hypoxia or in situ normoxia: The stem cell paradigm. *J Cell Physiol*. 219:271-275.

Jablonska, B., J. Scafidi, A. Aguirre, F. Vaccarino, V. Nguyen, E. Borok, T.L. Horvath, D.H. Rowitch, and V. Gallo. 2012. Oligodendrocyte regeneration after neonatal hypoxia requires FoxO1-mediated p27Kip1 expression. *J Neurosci*. 32:14775-14793.

Kung, A.L., S.D. Zabludoff, D.S. France, S.J. Freedman, E.A. Tanner, A. Vieira, S. Cornell-Kennon, J. Lee, B. Wang, J. Wang, K. Memmert, H.U. Naegeli, F. Petersen, M.J. Eck, K.W. Bair, A.W. Wood, and D.M. Livingston. 2004. Small molecule blockade of transcriptional coactivation of the hypoxia-inducible factor pathway. *Cancer Cell*. 6:33-43.

Lang, J., Y. Maeda, P. Bannerman, J. Xu, M. Horiuchi, D. Pleasure, and F. Guo. 2013. Adenomatous polyposis coli regulates oligodendroglial development. *The Journal of neuroscience : the official journal of the Society for Neuroscience*. 33:3113-3130.

Lappe-Siefke, C., S. Goebbels, M. Gravel, E. Nicksch, J. Lee, P.E. Braun, I.R. Griffiths, and K.A. Nave. 2003. Disruption of Cnp1 uncouples oligodendroglial functions in axonal support and myelination. *Nat Genet*. 33:366-374.

Lee, H.K., L.S. Chaboub, W. Zhu, D. Zollinger, M.N. Rasband, S.P. Fancy, and B. Deneen. 2015a. Daam2-PIP5K Is a Regulatory Pathway for Wnt Signaling and Therapeutic Target for Remyelination in the CNS. *Neuron*. 85:1227-1243.

Lee, H.K., D. Laug, W. Zhu, J.M. Patel, K. Ung, B.R. Arenkiel, S.P. Fancy, C. Mohila, and B. Deneen. 2015b. Apcdd1 stimulates oligodendrocyte differentiation after white matter injury. *Glia*. 63:1840-1849.

Li, L., K.M. Candelario, K. Thomas, R. Wang, K. Wright, A. Messier, and L.A. Cunningham. 2014. Hypoxia inducible factor-1alpha (HIF-1alpha) is required for neural stem cell maintenance and vascular stability in the adult mouse SVZ. *J Neurosci*. 34:16713-16719.

Liu, W., Y. Shen, J.M. Plane, D.E. Pleasure, and W. Deng. 2011. Neuroprotective potential of erythropoietin and its derivative carbamylated erythropoietin in periventricular leukomalacia. *Exp Neurol*. 230:227-239.

Liu, X.B., Y. Shen, J.M. Plane, and W. Deng. 2013. Vulnerability of premyelinating oligodendrocytes to white-matter damage in neonatal brain injury. *Neurosci Bull*. 29:229-238.

Milosevic, J., M. Maisel, F. Wegner, J. Leuchtenberger, R.H. Wenger, M. Gerlach, A. Storch, and J. Schwarz. 2007. Lack of hypoxia-inducible factor-1 alpha impairs midbrain neural precursor cells involving vascular endothelial growth factor signaling. *J Neurosci*. 27:412-421.

Moyon, S., J.L. Huynh, D. Dutta, F. Zhang, D. Ma, S. Yoo, R. Lawrence, M. Wegner, G.R. John, B. Emery, C. Lubetzki, R.J. Franklin, G. Fan, J. Zhu, J.L. Dupree, and P. Casaccia. 2016. Functional Characterization of DNA Methylation in the Oligodendrocyte Lineage. *Cell Rep*.

Puri, S., H. Akiyama, and M. Hebrok. 2013. VHL-mediated disruption of Sox9 activity compromises beta-cell identity and results in diabetes mellitus. *Genes Dev*. 27:2563-2575.

Reiprich, S., M. Cantone, M. Weider, T. Baroti, J. Wittstatt, C. Schmitt, M. Kuspert, J. Vera, and M. Wegner. 2017. Transcription factor Sox10 regulates oligodendroglial Sox9 levels via microRNAs. *Glia*. 65:1089-1102.

Scott, C.E., S.L. Wynn, A. Sesay, C. Cruz, M. Cheung, M.V. Gomez Gaviro, S. Booth, B. Gao, K.S. Cheah, R. Lovell-Badge, and J. Briscoe. 2010. SOX9 induces and maintains neural stem cells. *Nat Neurosci*. 13:1181-1189.

Semenza, G.L. 2012. Hypoxia-inducible factors in physiology and medicine. *Cell*. 148:399-408.

Semple, B.D., K. Blomgren, K. Gimlin, D.M. Ferriero, and L.J. Noble-Haeusslein. 2013. Brain development in rodents and humans: Identifying benchmarks of maturation and vulnerability to injury across species. *Prog Neurobiol*. 106-107:1-16.

Sharp, F.R., and M. Bernaudin. 2004. HIF1 and oxygen sensing in the brain. *Nat Rev Neurosci*. 5:437-448.

Shen, Y., J.M. Plane, and W. Deng. 2010. Mouse models of periventricular leukomalacia. *J Vis Exp*.

Stolt, C.C., P. Lommes, E. Sock, M.C. Chaboissier, A. Schedl, and M. Wegner. 2003. The Sox9 transcription factor determines glial fate choice in the developing spinal cord. *Genes Dev*. 17:1677-1689.

Sun, W., A. Cornwell, J. Li, S. Peng, M.J. Osorio, N. Aalling, S. Wang, A. Benraiss, N. Lou, S.A. Goldman, and M. Nedergaard. 2017. SOX9 Is an Astrocyte-Specific Nuclear Marker in the Adult Brain Outside the Neurogenic Regions. *J Neurosci*. 37:4493-4507.

Tomita, S., M. Ueno, M. Sakamoto, Y. Kitahama, M. Ueki, N. Maekawa, H. Sakamoto, M. Gassmann, R. Kageyama, N. Ueda, F.J. Gonzalez, and Y. Takahama. 2003. Defective brain development in mice lacking the Hif-1alpha gene in neural cells. *Mol Cell Biol*. 23:6739-6749.

Viziteu, E., C. Grandmougin, H. Goldschmidt, A. Seckinger, D. Hose, B. Klein, and J. Moreaux. 2016. Chetomin, targeting HIF-1 alpha/p300 complex, exhibits antitumour activity in multiple myeloma. *Brit J Cancer*. 114:519-523.

Voelker, C.C., N. Garin, J.S. Taylor, B.H. Gahwiler, J.P. Hornung, and Z. Molnar. 2004. Selective neurofilament (SMI-32, FNP-7 and N200) expression in subpopulations of layer V pyramidal neurons in vivo and in vitro. *Cereb Cortex*. 14:1276-1286.

Volpe, J.J. 2009. Brain injury in premature infants: a complex amalgam of destructive and developmental disturbances. *Lancet Neurol*. 8:110-124.

Ye, F., Y. Chen, T. Hoang, R.L. Montgomery, X.H. Zhao, H. Bu, T. Hu, M.M. Taketo, J.H. van Es, H. Clevers, J. Hsieh, R. Bassel-Duby, E.N. Olson, and Q.R. Lu. 2009. HDAC1 and HDAC2 regulate oligodendrocyte differentiation by disrupting the beta-catenin-TCF interaction. *Nat Neurosci*. 12:829-838.

Yuen, T.J., J.C. Silbereis, A. Griveau, S.M. Chang, R. Daneman, S.P. Fancy, H. Zahed, E. Maltepe, and D.H. Rowitch. 2014. Oligodendrocyte-Encoded HIF Function Couples Postnatal Myelination and White Matter Angiogenesis. *Cell*. 158:383-396.

Zhang, K., L. Zhu, and M. Fan. 2011. Oxygen, a Key Factor Regulating Cell Behavior during Neurogenesis and Cerebral Diseases. *Front Mol Neurosci*. 4:5.

Zhang, S., A. Rasai, Y. Wang, J. Xu, P. Bannerman, D. Erol, D. Tsegaye, A. Wang, A. Soulika, X. Zhan, and F. Guo. 2018a. The Stem Cell Factor Sox2 Is a Positive Timer of Oligodendrocyte Development in the Postnatal Murine Spinal Cord. *Mol Neurobiol*.

Zhang, S., X. Zhu, X. Gui, C. Croteau, L. Song, J. Xu, A. Wang, P. Bannerman, and F. Guo. 2018b. Sox2 is essential for oligodendroglial proliferation and differentiation during postnatal brain myelination and CNS remyelination. *J Neurosci*.

Zhang, Y., K. Chen, S.A. Sloan, M.L. Bennett, A.R. Scholze, S. O'Keeffe, H.P. Phatnani, P. Guarnieri, C. Caneda, N. Ruderisch, S. Deng, S.A. Liddelow, C. Zhang, R. Daneman, T. Maniatis, B.A. Barres, and J.Q. Wu. 2014. An RNA-sequencing transcriptome and splicing database of glia, neurons, and vascular cells of the cerebral cortex. *The Journal of neuroscience : the official journal of the Society for Neuroscience*. 34:11929-11947.

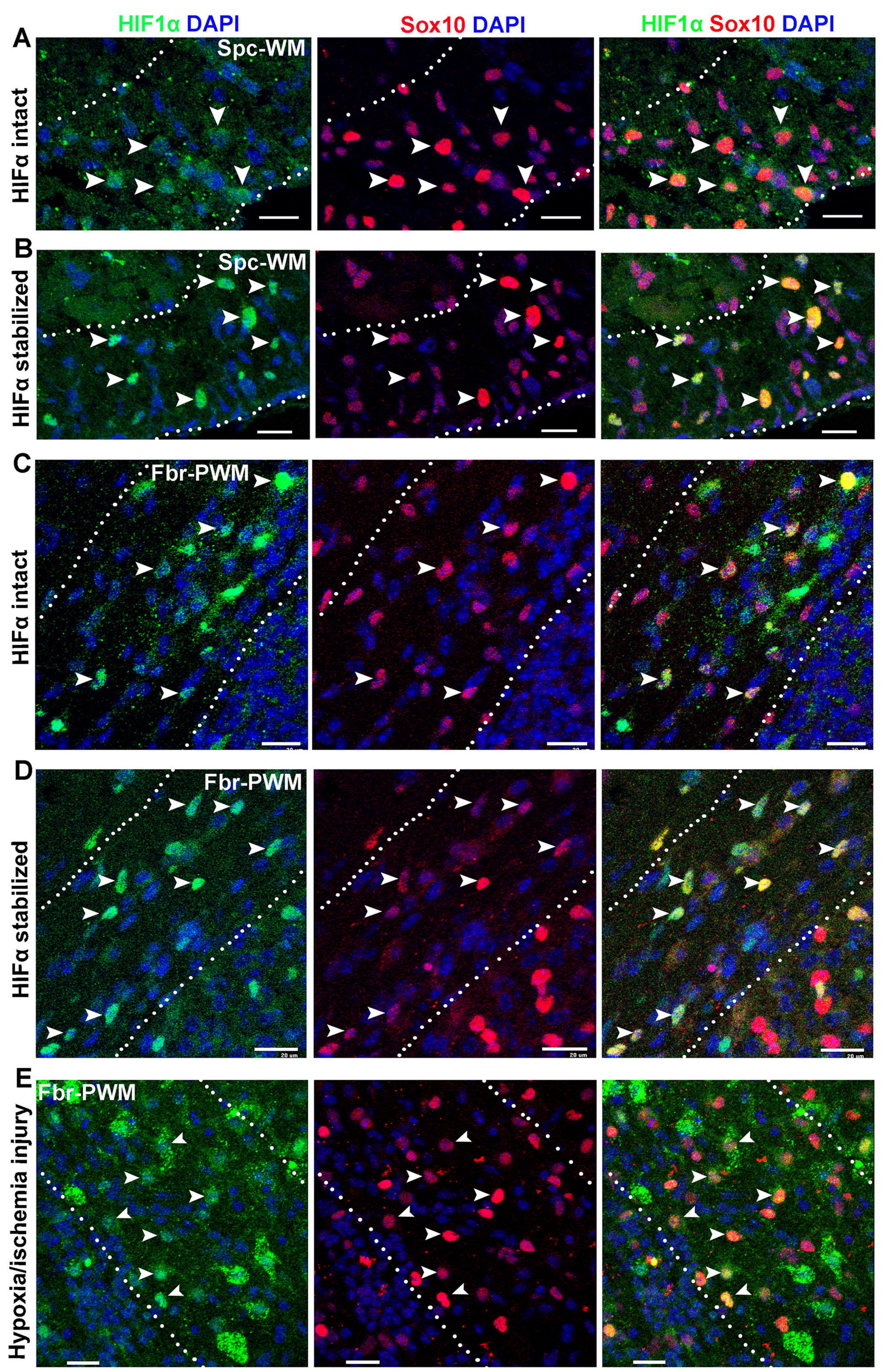
HIF1α DAPI
Sox10 DAPI
HIF1α Sox10 DAPI
A
Spc-WM
HIFα intact
B
Spc-WM
HIFα stabilized
C
Fbr-PWM
HIFα intact
D
Fbr-PWM
HIFα stabilized
E
Fbr-PWM
Hypoxia/ischemia injury

Pdgfrα-CreER^{T2}:Hif1α$^{fl/fl}$:Hif2α$^{fl/fl}$ (PDGFRα:HIFα cKO) and non-Cre Ctrl

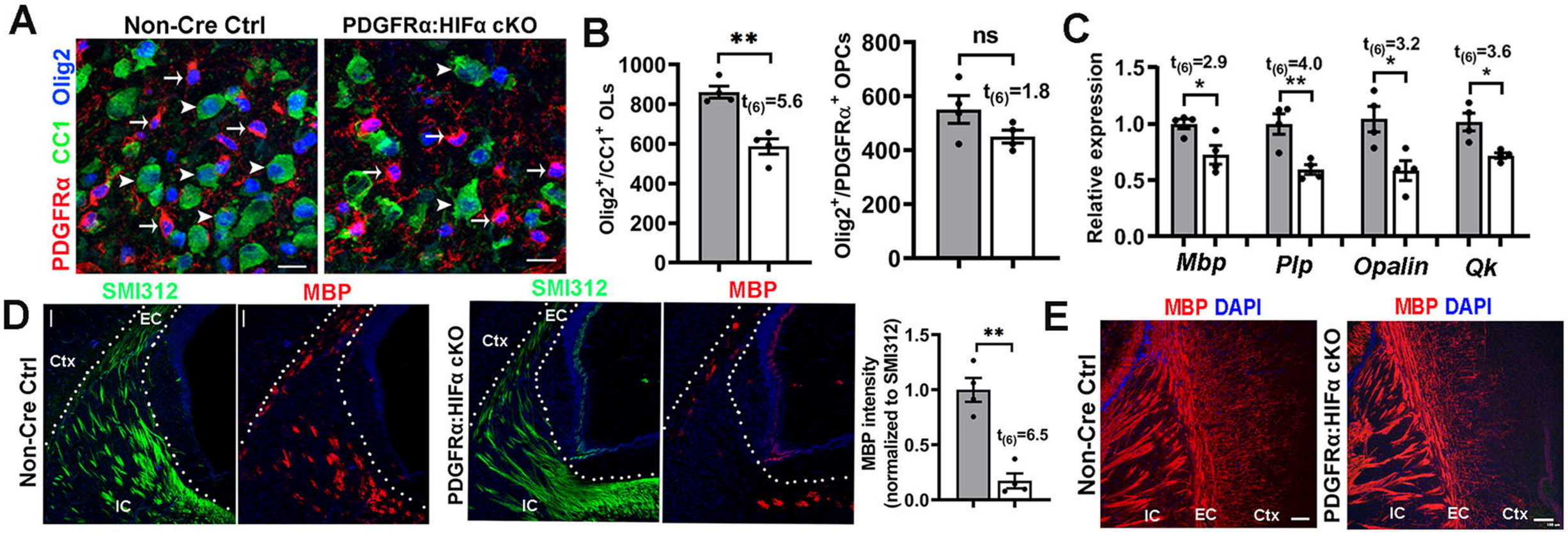

Cnp-Cre:Hif1α$^{fl/fl}$:Hif2α$^{fl/fl}$ (Cnp:HIFα cKO) and non-Cre Ctrl

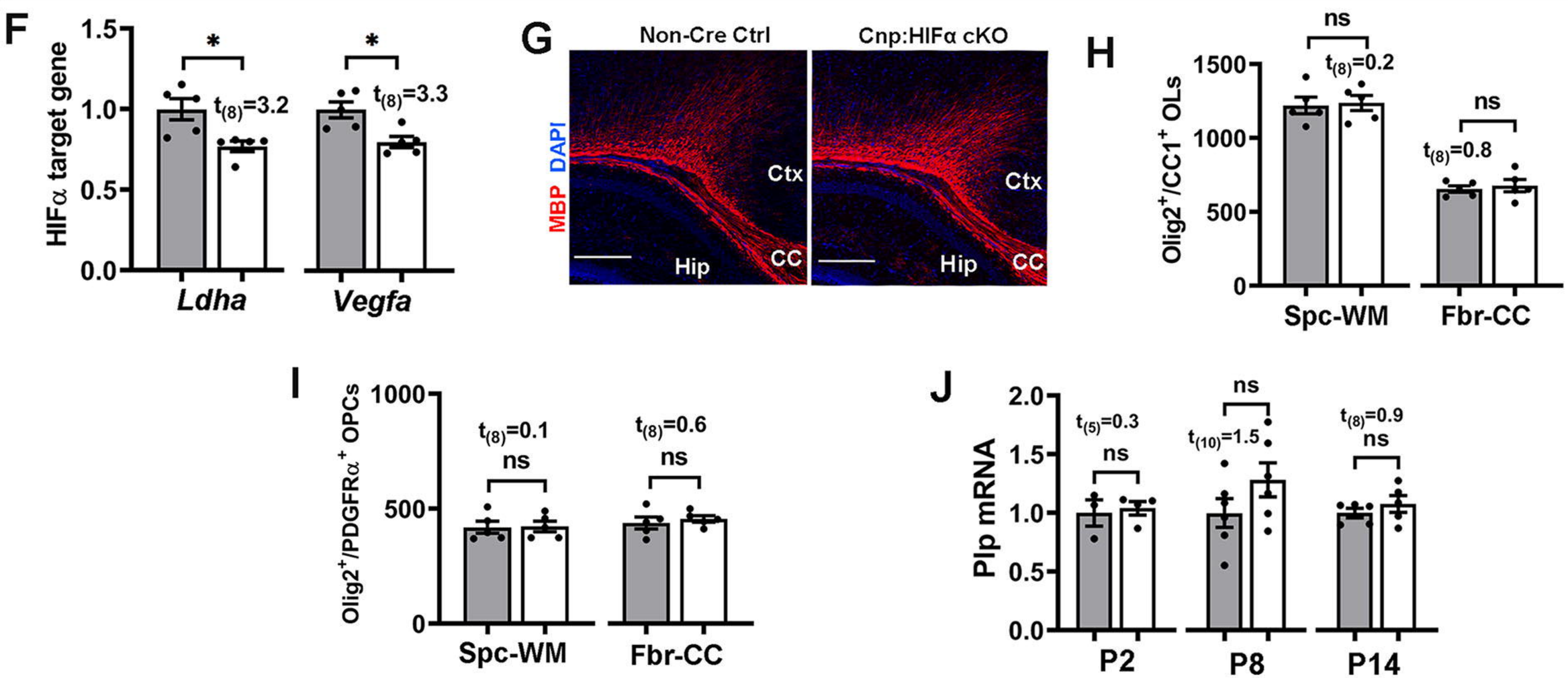

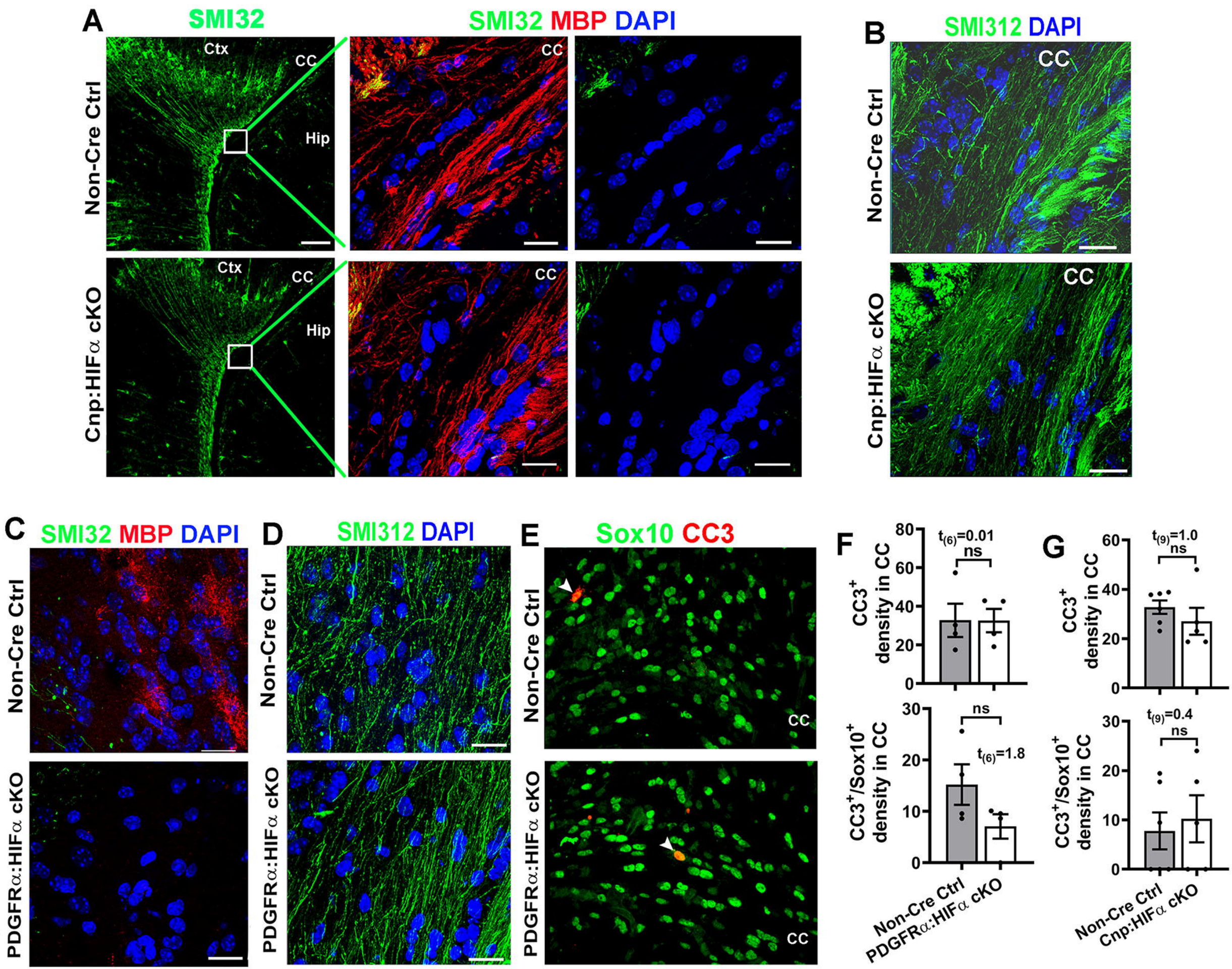
A
SMI32
SMI32 MBP DAPI
Non-Cre Ctrl
Cnp:HIFα cKO
Ctx
CC
Hip
B
SMI312 DAPI
C
SMI32 MBP DAPI
PDGFRα:HIFα cKO
D
SMI312 DAPI
E
Sox10 CC3
F
CC3+ density in CC
t(6)=0.01
ns
CC3+/Sox10+ density in CC
t(6)=1.8
G
t(9)=1.0
t(9)=0.4
Non-Cre Ctrl
PDGFRα:HIFα cKO
Cnp:HIFα cKO

Sox10-Cre:Vhl$^{fl/fl}$ (Sox10:VHL cKO) and non-Cre Ctrl

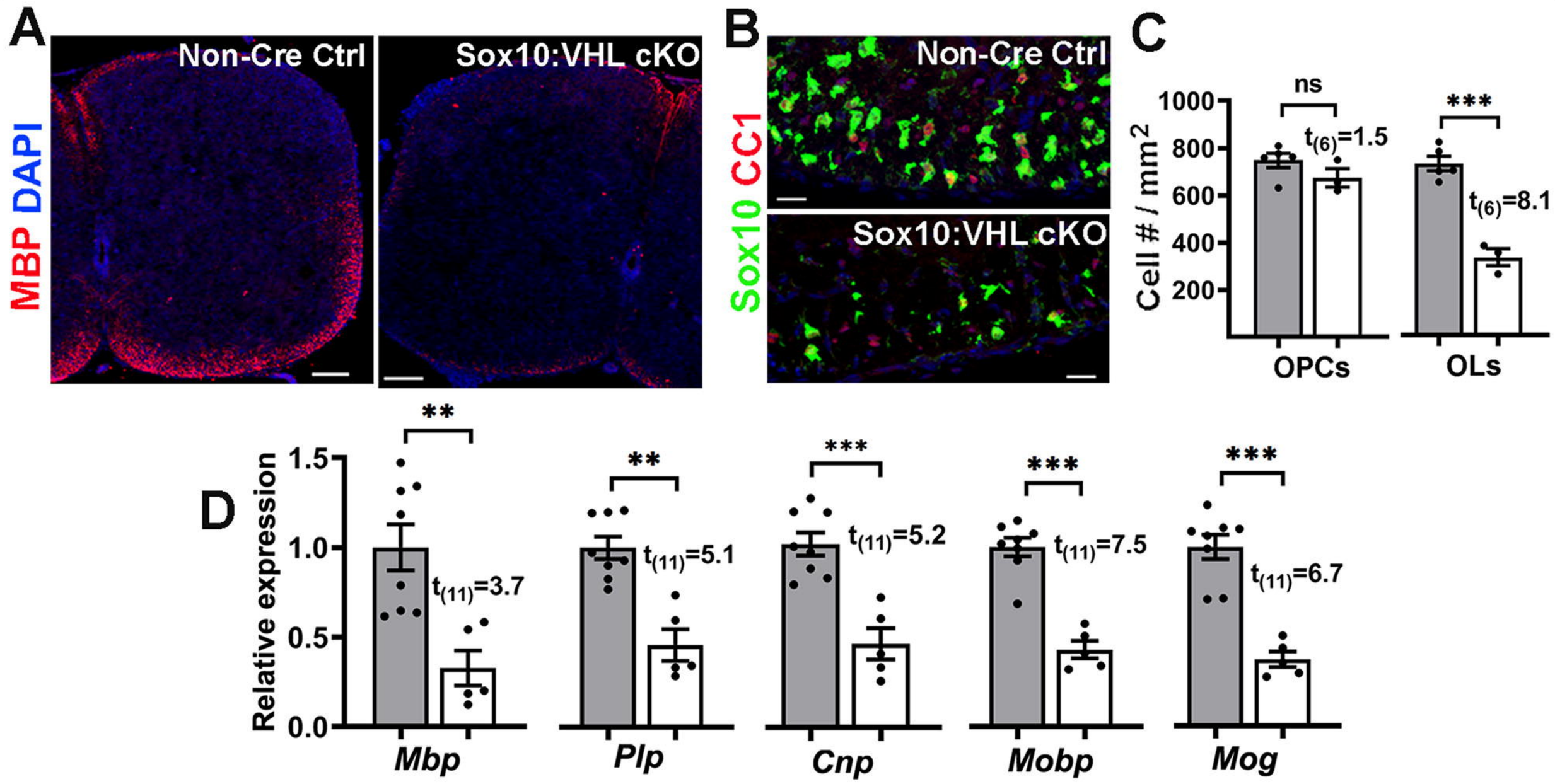

Cnp-Cre:Vhl$^{fl/fl}$ (Cnp:VHL cKO) and non-Cre Ctrl

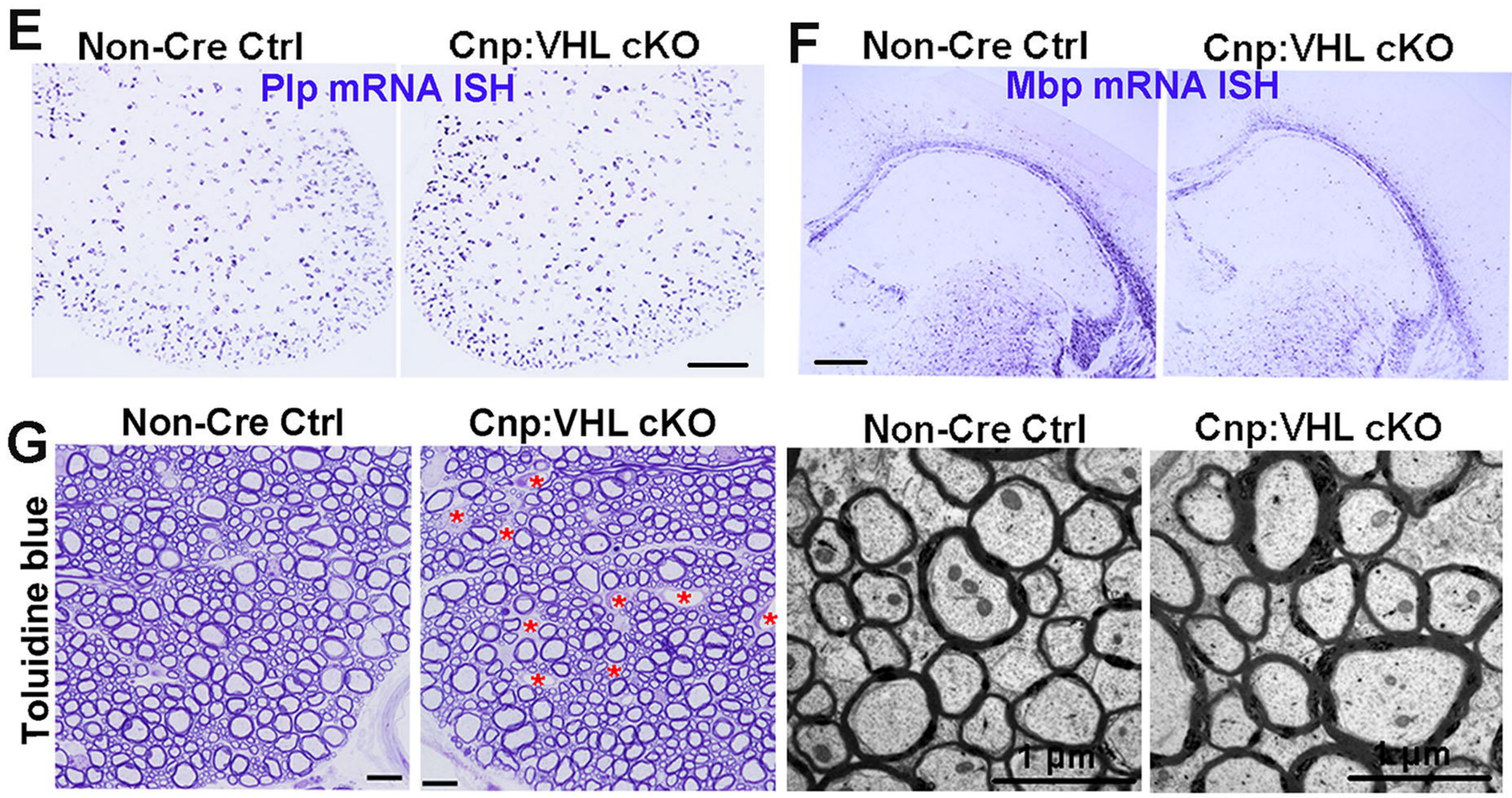

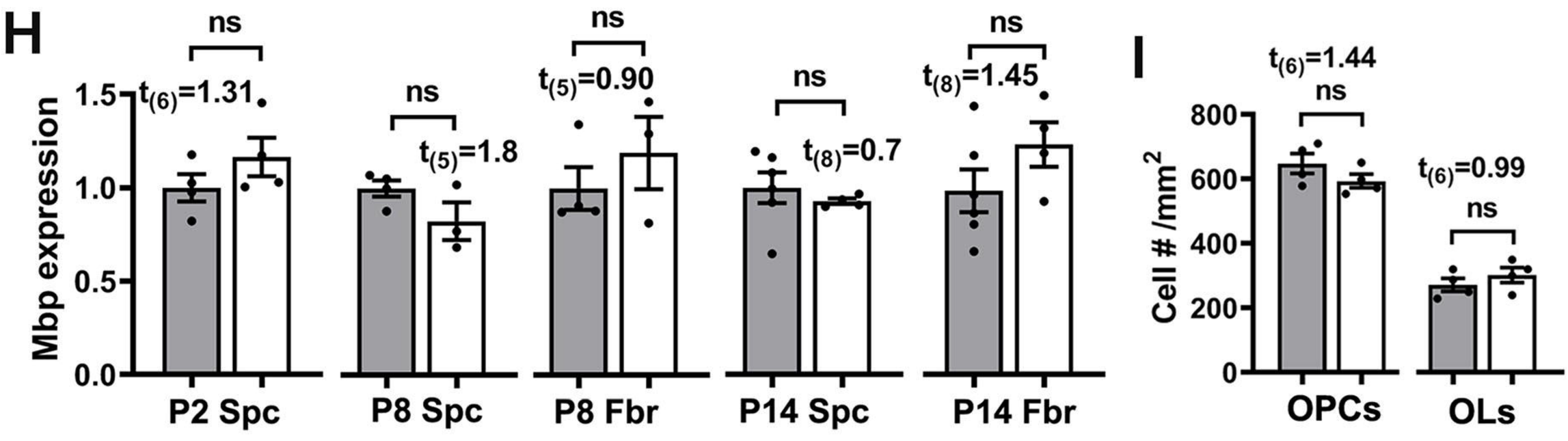

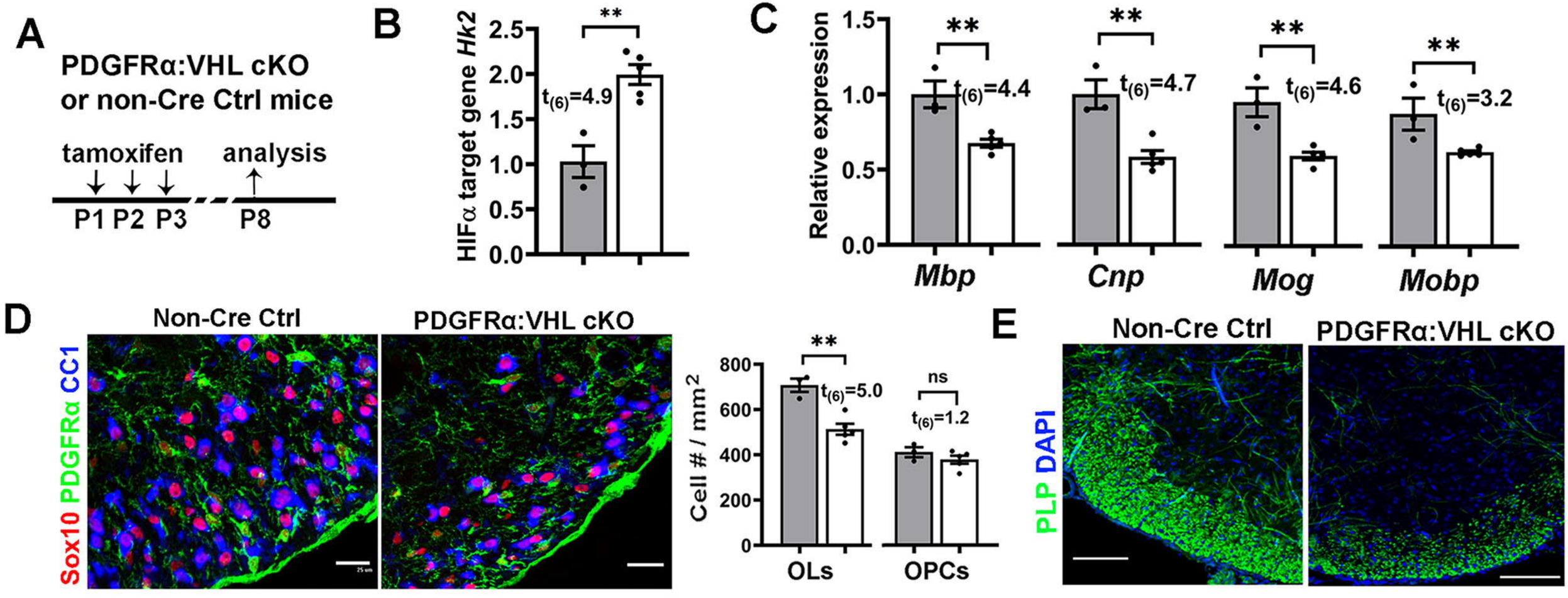
A
PDGFRα:VHL cKO
or non-Cre Ctrl mice
tamoxifen
analysis
P1 P2 P3
P8
B
HIFα target gene Hk2
2.5
2.0
1.5
1.0
0.5
0.0
**
t(6)=4.9
C
Relative expression
1.5
1.0
0.5
0.0
**
t(6)=4.4
t(6)=4.7
t(6)=4.6
t(6)=3.2
Mbp
Cnp
Mog
Mobp
D
Non-Cre Ctrl
PDGFRα:VHL cKO
Sox10 PDGFRα CC1
Cell # / mm2
800
600
400
200
0
**
t(6)=5.0
ns
t(6)=1.2
OLs
OPCs
E
Non-Cre Ctrl
PDGFRα:VHL cKO
PLP DAPI

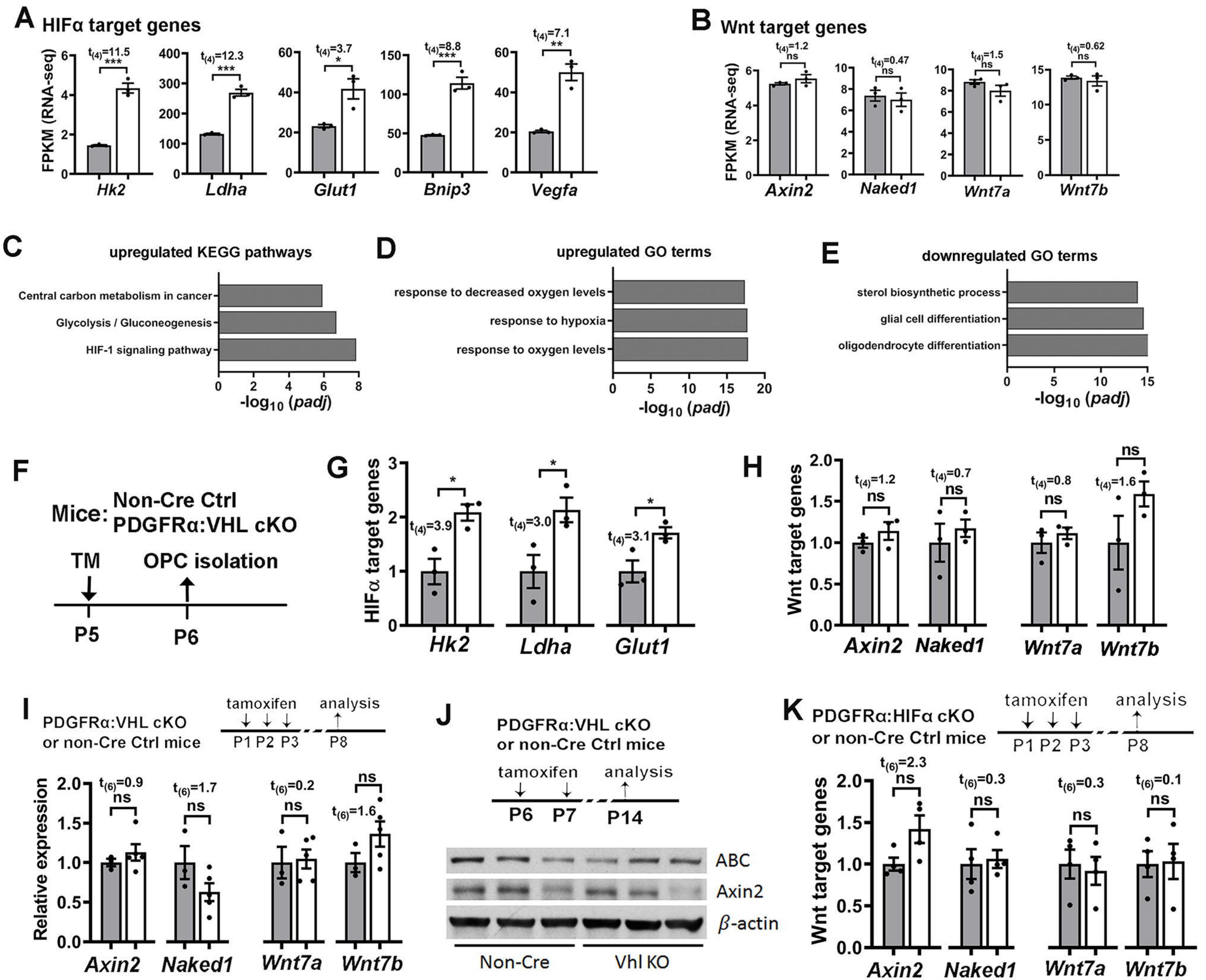
A
HIFα target genes
FPKM (RNA-seq)
Hk2
Ldha
Glut1
Bnip3
Vegfa
B
Wnt target genes
Axin2
Naked1
Wnt7a
Wnt7b
C
upregulated KEGG pathways
Central carbon metabolism in cancer
Glycolysis / Gluconeogenesis
HIF-1 signaling pathway
-log10 (padj)
D
upregulated GO terms
response to decreased oxygen levels
response to hypoxia
response to oxygen levels
E
downregulated GO terms
sterol biosynthetic process
glial cell differentiation
oligodendrocyte differentiation
F
Mice: Non-Cre Ctrl
PDGFRα:VHL cKO
TM
OPC isolation
P5
P6
G
HIFα target genes
H
Wnt target genes
I
PDGFRα:VHL cKO
or non-Cre Ctrl mice
tamoxifen
analysis
P1 P2 P3
P8
Relative expression
J
PDGFRα:VHL cKO
or non-Cre Ctrl mice
tamoxifen
analysis
P6 P7
P14
ABC
Axin2
β-actin
Non-Cre
Vhl KO
K
PDGFRα:HIFα cKO
or non-Cre Ctrl mice
tamoxifen
analysis
P1 P2 P3
P8
Wnt target genes

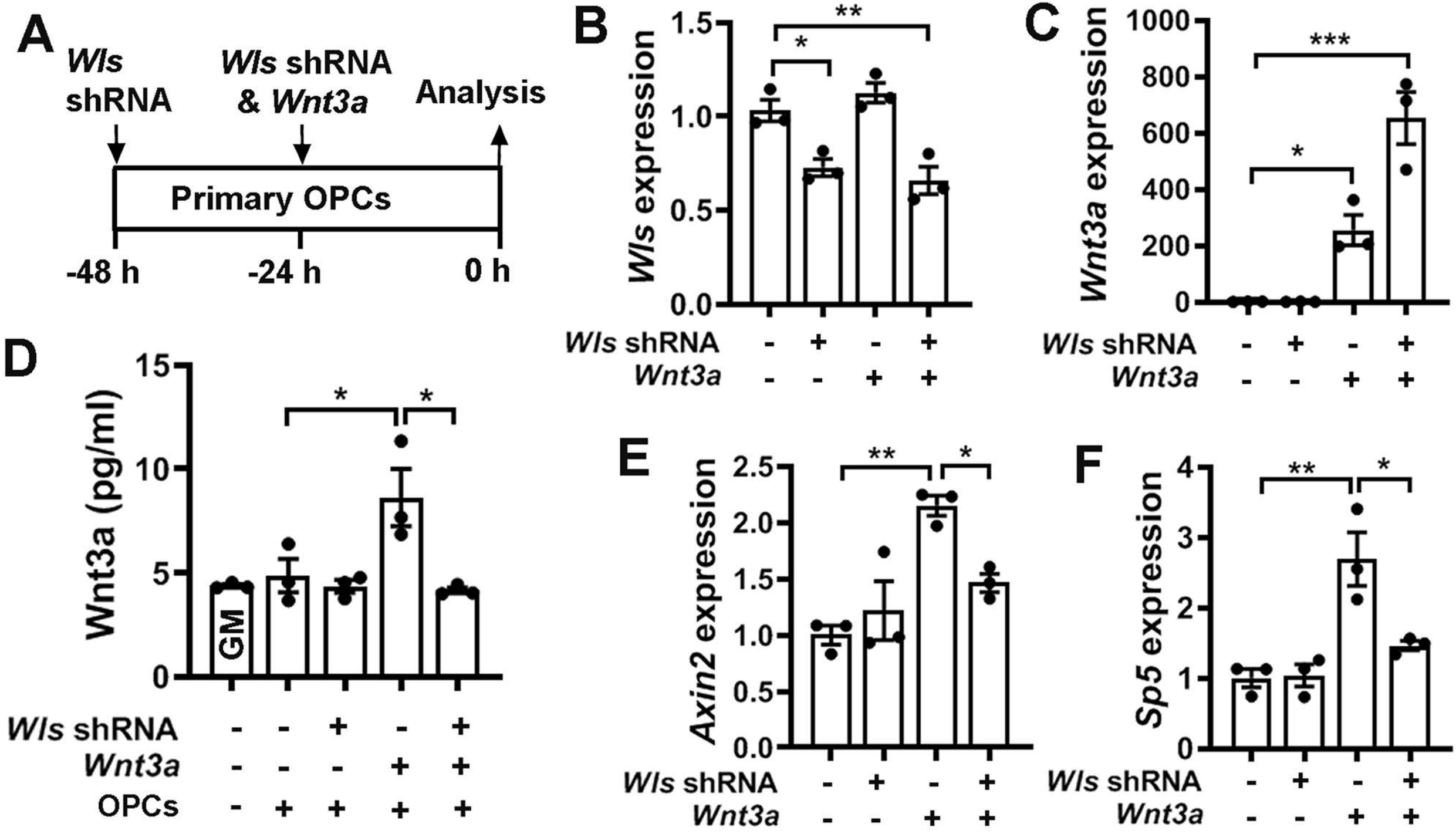
A
Wls shRNA
Wls shRNA & Wnt3a
Analysis
Primary OPCs
-48 h
-24 h
0 h
B
Wls expression
1.5
1.0
0.5
0.0
*
**
Wls shRNA - + - +
Wnt3a - - + +
C
Wnt3a expression
1000
800
600
400
200
0
*
***
Wls shRNA - + - +
Wnt3a - - + +
D
Wnt3a (pg/ml)
15
10
5
0
GM
*
*
Wls shRNA - - + - +
Wnt3a - - - + +
OPCs - + + + +
E
Axin2 expression
2.5
2.0
1.5
1.0
0.5
0.0
**
*
Wls shRNA - + - +
Wnt3a - - + +
F
Sp5 expression
4
3
2
1
0
**
*
Wls shRNA - + - +
Wnt3a - - + +

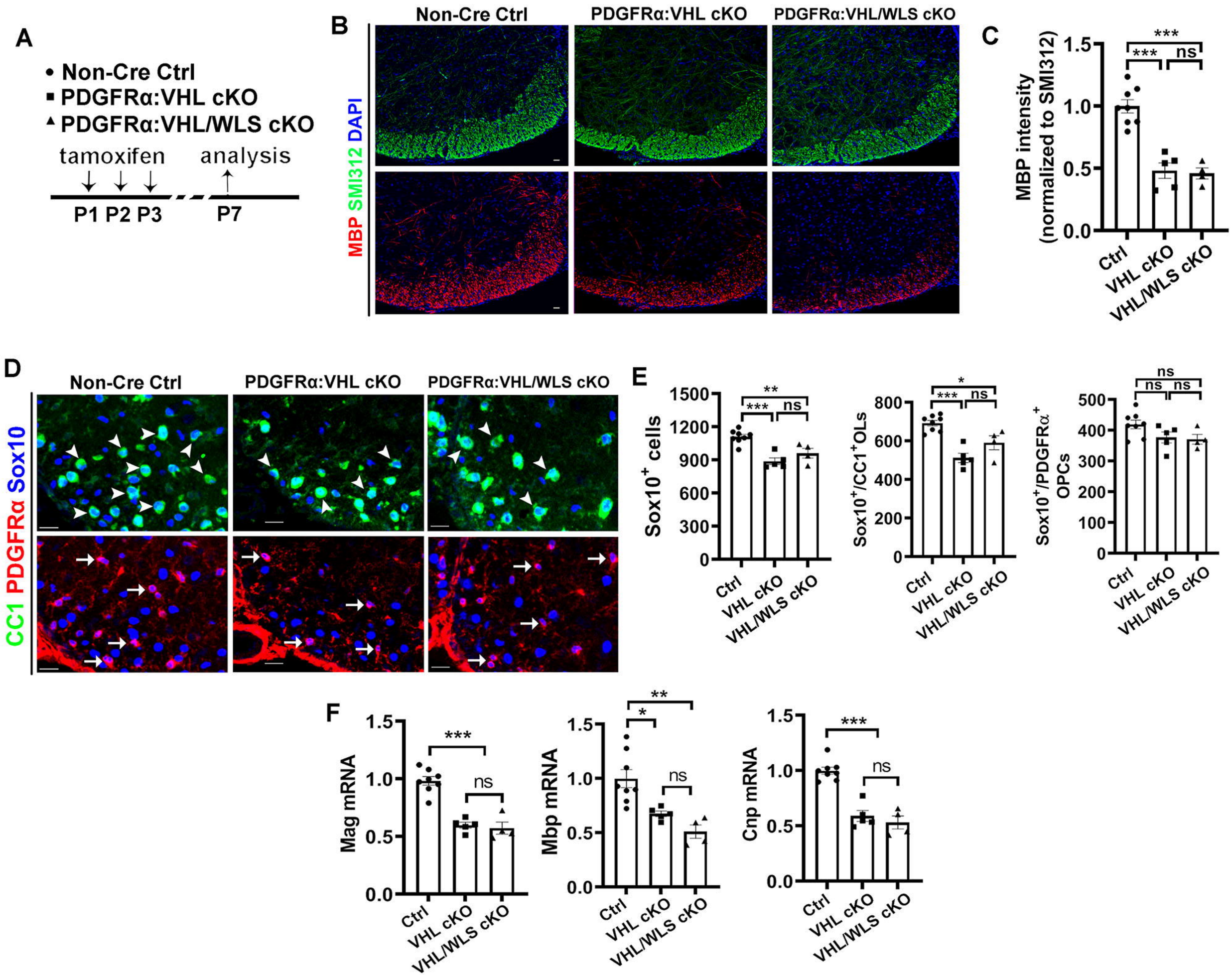
A
Non-Cre Ctrl
PDGFRα:VHL cKO
PDGFRα:VHL/WLS cKO
tamoxifen
analysis
P1 P2 P3
P7
B
Non-Cre Ctrl
PDGFRα:VHL cKO
PDGFRα:VHL/WLS cKO
MBP SMI312 DAPI
C
MBP intensity (normalized to SMI312)
1.5
1.0
0.5
0.0
***
***
ns
Ctrl
VHL cKO
VHL/WLS cKO
D
Non-Cre Ctrl
PDGFRα:VHL cKO
PDGFRα:VHL/WLS cKO
CC1 PDGFRα Sox10
E
Sox10+ cells
1500
1200
900
600
300
0
**
***
ns
Sox10+/CC1+OLs
800
600
400
200
0
*
***
ns
Sox10+/PDGFRα+ OPCs
500
400
300
200
100
0
ns
ns
ns
Ctrl
VHL cKO
VHL/WLS cKO
F
Mag mRNA
1.5
1.0
0.5
0.0
***
ns
Mbp mRNA
1.5
1.0
0.5
0.0
**
*
ns
Cnp mRNA
1.5
1.0
0.5
0.0
***
ns
Ctrl
VHL cKO
VHL/WLS cKO

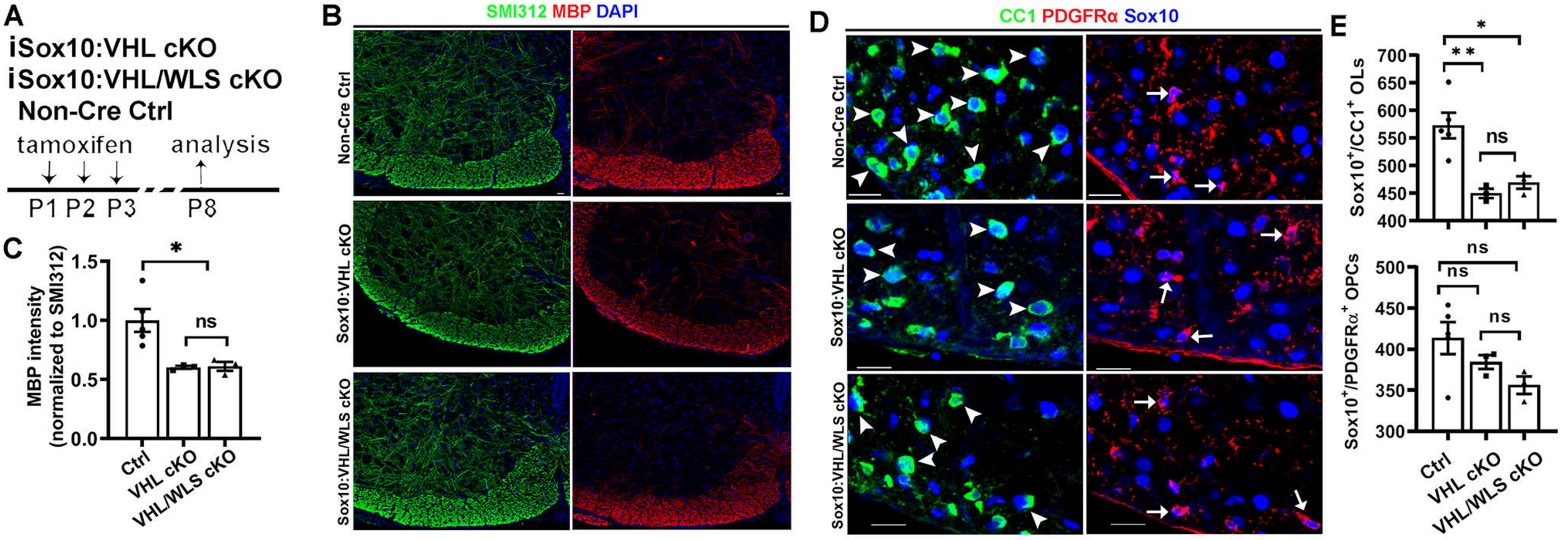
A
iSox10:VHL cKO
iSox10:VHL/WLS cKO
Non-Cre Ctrl
tamoxifen
analysis
P1 P2 P3
P8
B
SMI312 MBP DAPI
Non-Cre Ctrl
Sox10:VHL cKO
Sox10:VHL/WLS cKO
C
MBP intensity (normalized to SMI312)
1.5
1.0
0.5
0.0
*
ns
Ctrl
VHL cKO
VHL/WLS cKO
D
CC1 PDGFRα Sox10
Non-Cre Ctrl
Sox10:VHL cKO
Sox10:VHL/WLS cKO
E
Sox10+/CC1+ OLs
700
650
600
550
500
450
400
*
**
ns
Sox10+/PDGFRα+ OPCs
500
450
400
350
300
ns
ns
ns
Ctrl
VHL cKO
VHL/WLS cKO

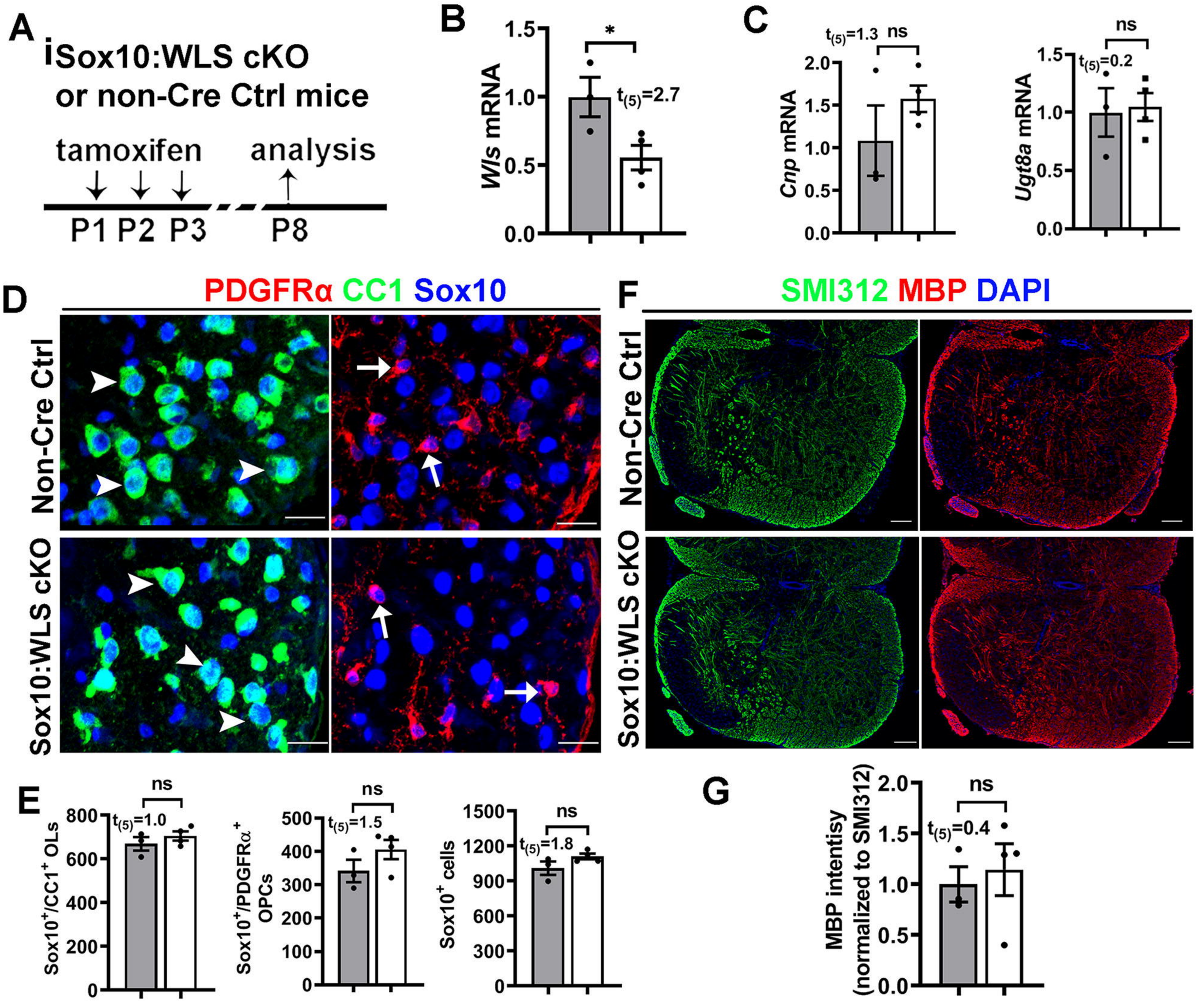
A
iSox10:WLS cKO
or non-Cre Ctrl mice
tamoxifen
analysis
P1 P2 P3
P8
B
Wls mRNA
1.5
1.0
0.5
0.0
*
t(5)=2.7
C
Cnp mRNA
t(5)=1.3
ns
2.0
1.5
1.0
0.5
0.0
Ugt8a mRNA
ns
t(5)=0.2
1.5
1.0
0.5
0.0
D
PDGFRα CC1 Sox10
Non-Cre Ctrl
Sox10:WLS cKO
F
SMI312 MBP DAPI
Non-Cre Ctrl
Sox10:WLS cKO
E
Sox10+/CC1+ OLs
ns
t(5)=1.0
800
600
400
200
0
Sox10+/PDGFRα+ OPCs
ns
t(5)=1.5
500
400
300
200
100
0
Sox10+ cells
ns
t(5)=1.8
1500
1200
900
600
300
0
G
MBP intentisy (normalized to SMI312)
ns
t(5)=0.4
2.0
1.5
1.0
0.5
0.0

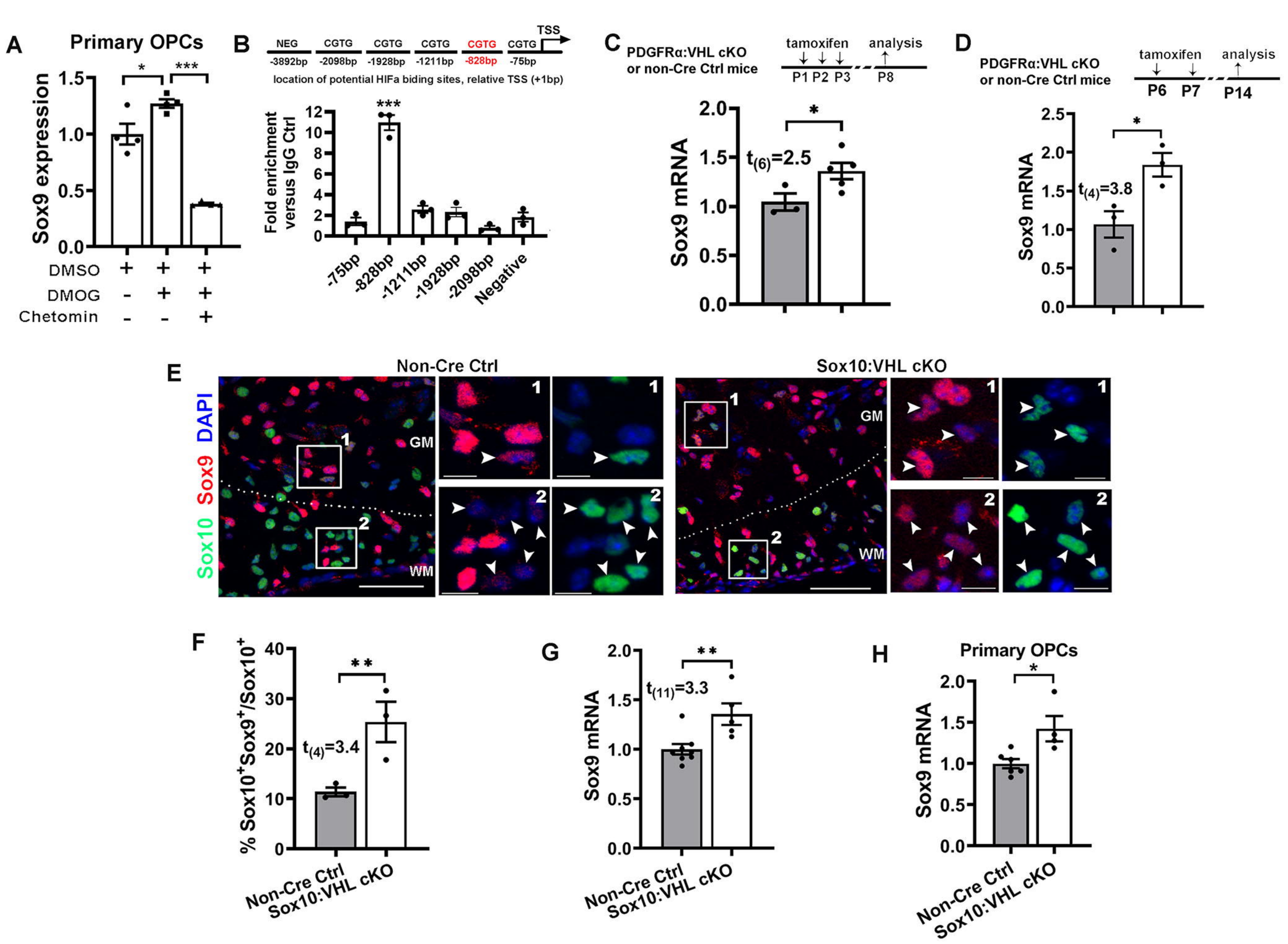
A
Primary OPCs
Sox9 expression
DMSO
DMOG
Chetomin
B
NEG
CGTG
TSS
-3892bp
-2098bp
-1928bp
-1211bp
-828bp
-75bp
location of potential HIFa biding sites, relative TSS (+1bp)
Fold enrichment versus IgG Ctrl
-75bp
-828bp
-1211bp
-1928bp
-2098bp
Negative
C
PDGFRα:VHL cKO or non-Cre Ctrl mice
tamoxifen
analysis
P1 P2 P3
P8
Sox9 mRNA
t(6)=2.5
D
PDGFRα:VHL cKO or non-Cre Ctrl mice
tamoxifen
analysis
P6 P7
P14
Sox9 mRNA
t(4)=3.8
E
Non-Cre Ctrl
Sox10:VHL cKO
DAPI
Sox9
Sox10
GM
WM
F
% Sox10+Sox9+/Sox10+
t(4)=3.4
Non-Cre Ctrl
Sox10:VHL cKO
G
Sox9 mRNA
t(11)=3.3
Non-Cre Ctrl
Sox10:VHL cKO
H
Primary OPCs
Sox9 mRNA
Non-Cre Ctrl
Sox10:VHL cKO

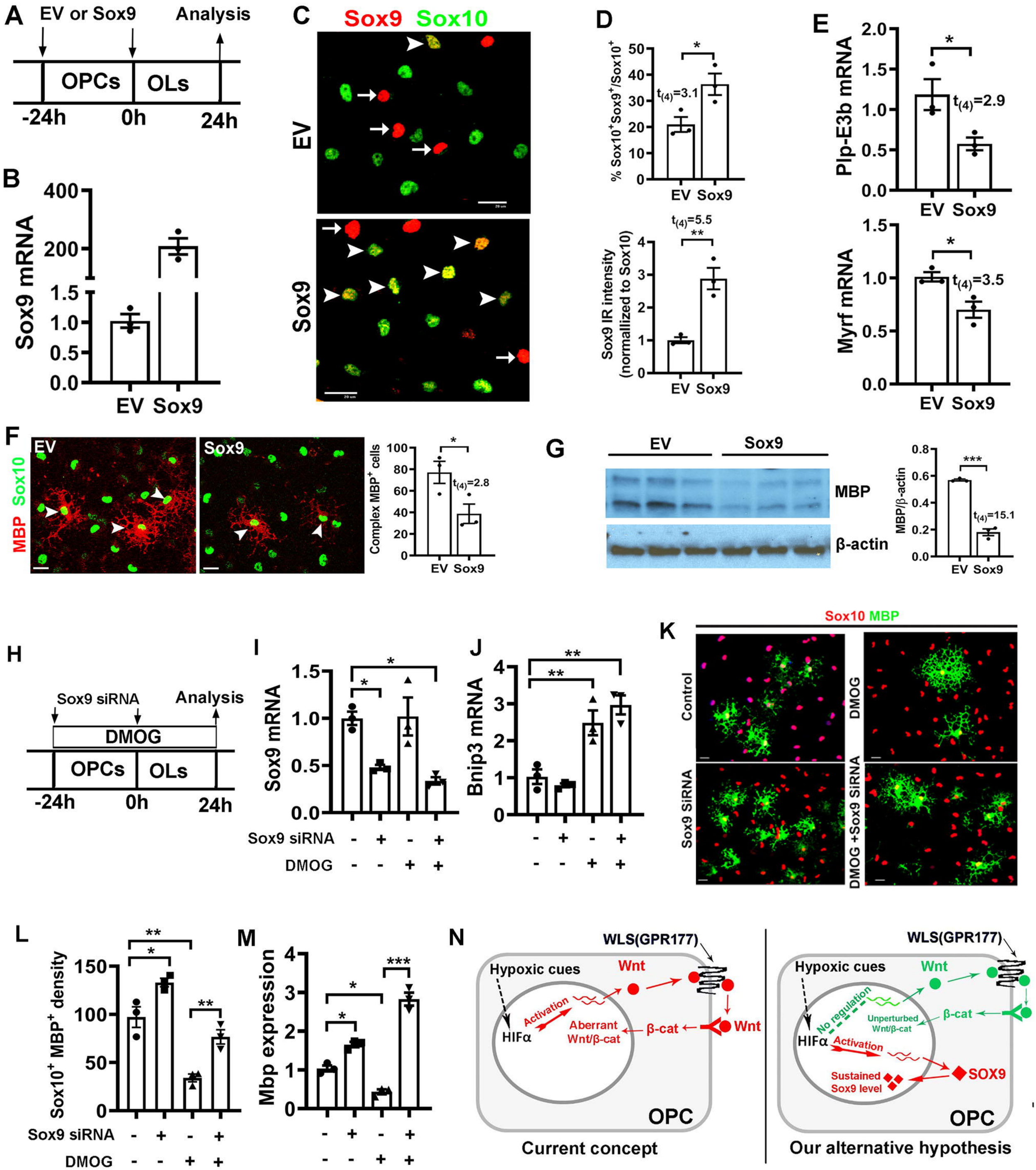
A
EV or Sox9
Analysis
OPCs
OLs
-24h
0h
24h
B
Sox9 mRNA
EV
Sox9
C
Sox9
Sox10
EV
Sox9
D
% Sox10+Sox9+/Sox10+
t(4)=3.1
Sox9 IR intensity (normallized to Sox10)
t(4)=5.5
E
Plp-E3b mRNA
t(4)=2.9
Myrf mRNA
t(4)=3.5
F
EV
Sox9
MBP
Sox10
Complex MBP+ cells
t(4)=2.8
G
EV
Sox9
MBP
β-actin
MBP/β-actin
t(4)=15.1
H
Sox9 siRNA
Analysis
DMOG
OPCs
OLs
-24h
0h
24h
I
Sox9 mRNA
Sox9 siRNA
DMOG
J
Bnip3 mRNA
K
Sox10 MBP
Control
DMOG
Sox9 SiRNA
DMOG +Sox9 SiRNA
L
Sox10+ MBP+ density
Sox9 siRNA
DMOG
M
Mbp expression
N
WLS(GPR177)
Hypoxic cues
Wnt
Activation
HIFα
Aberrant Wnt/β-cat
β-cat
Wnt
OPC
Current concept
WLS(GPR177)
Hypoxic cues
Wnt
No regulation
Unperturbed Wnt/β-cat
β-cat
HIFα
Activation
Sustained Sox9 level
SOX9
OPC
Our alternative hypothesis